nature neuroscience

ARTICLES

https://doi.org/10.1038/s41593-020-0620-z

Associative and plastic thalamic signaling to the lateral amygdala controls fear behavior

Boglárka Barsy[1,9], Kinga Kocsis[1,2,9], Aletta Magyar[1,3], Ákos Babiczky[1,4], Mónika Szabó[1,3], Judit M. Veres[1], Dániel Hillier[5,6], István Ulbert[5,6], Ofer Yizhar[7] and Ferenc Mátyás[1,8]✉

Decades of research support the idea that associations between a conditioned stimulus (CS) and an unconditioned stimulus (US) are encoded in the lateral amygdala (LA) during fear learning. However, direct proof for the sources of CS and US information is lacking. Definitive evidence of the LA as the primary site for cue association is also missing. Here, we show that calretinin (Calr)-expressing neurons of the lateral thalamus (Calr$^+$LT neurons) convey the association of fast CS (tone) and US (foot shock) signals upstream from the LA in mice. Calr$^+$LT input shapes a short-latency sensory-evoked activation pattern of the amygdala via both feedforward excitation and inhibition. Optogenetic silencing of Calr$^+$LT input to the LA prevents auditory fear conditioning. Notably, fear conditioning drives plasticity in Calr$^+$LT neurons, which is required for appropriate cue and contextual fear memory retrieval. Collectively, our results demonstrate that Calr$^+$LT neurons provide integrated CS–US representations to the LA that support the formation of aversive memories.

Environmental cues that become affectively salient during learning must be processed with high efficacy to promote adaptation and survival. However, the circuit mechanisms for evolutionarily conserved and subconscious processing of these stimuli have not yet been fully established. The LA is considered to be the key brain region that processes associative fear memories by coupling a neutral sensory cue (a CS; for example, tone) with an affective (unconditioned) stimulus (US; for example, foot shock) during fear learning[1–3]. This association then drives the formation of a memory about the CS via synaptic changes in the LA[4]. As a consequence, the presentation of the same CS at a later time point elicits consistent fear responses. Contrary to current models, the source of the CS and US signals driving the memory processes are still unknown, and convincing evidence for signal association in the LA is lacking[5,6].

Given that in vivo recordings suggest that CS-related information reaches the amygdala with a short latency (<20 ms)[7], this process requires fast, probably subcortical, inputs to the LA. LT regions, namely the posterior intralaminar (PIL) and suprageniculate (SG) thalamic nuclei as well as the medial and dorsal parts of the medial geniculate thalamic nucleus (MGN (also called the medial geniculate body)), form direct functional connections with the LA[8]. However, because the medial part of the MGN (MGM) is part of the auditory thalamus, LT input to the LA is traditionally accepted as the major source of auditory CS[7,9]. Nevertheless, lesioning of these thalamic areas yielded contradictory findings regarding fear learning[9–11].

The source of US information in the LA that temporally matches the CS signal is also debated. Neurons in the parabrachial nucleus (PB)[12] and periaqueductal gray (PAG)[13,14] are activated by a US and affect fear learning. However, these nuclei cannot provide the LA with the short-latency US signal that is necessary for signal association (10–20 ms)[7], which is due to the lack of monosynaptic connections between the PB, PAG and the LA. The dorsomedial thalamic nuclei, including the paraventricular thalamus, can control fear memory formation and retrieval[15,16] by encoding arousal information[17] and stimulus salience[18]. Yet, this medial thalamic population mostly targets the basal amygdala (BA) and the central amygdala (CeA) and not the LA. Thus, it is still unclear how fast sensory (CS and US) input arrives to the LA and triggers association-driven learning.

Alternatively, the LA could receive US-related information directly from the above-mentioned lateral thalamic regions, which potentially convey a CS[19,20]. Although thalamic integration of a CS and a US was previously hypothesized[5], it has been mostly overlooked. Nevertheless, there is evidence to indicate that plasticity induced by auditory fear conditioning is present in these lateral thalamic regions[5,21].

On the basis of an anatomical exploration of direct midbrain inputs that predicted the responsiveness of these LT cells to auditory, visual and somatosensory signals[22,23], our aim was to assess whether the LT is able to integrate CS and US signals before the LA and transfer the association to its targets. In this study, we investigate the cellular origin, the modality of the encoded signal, the effector mechanism and the behavioral effects of LT projection to the LA during associative fear-learning in mice. Using a combination of cell-type-specific anatomical, optogenetic and in vivo electrophysiological approaches in an auditory fear-learning paradigm, we identified a direct glutamatergic LT pathway to the LA originating from Calr$^+$LT cells. These cells can form short-latency (<20 ms) CS–US associations upstream from the LA. This ability emerges from the ensemble of collicular, PAG and spinal trigeminal inputs that carry information about sensory and valence features of the environment. The Calr$^+$LT route transfers this associative

[1]Laboratory of Neuronal Network and Behavior, Institute of Cognitive Neuroscience and Psychology, Research Center for Natural Sciences, Budapest, Hungary. [2]Roska Tamás Doctoral School of Sciences and Technology, Faculty of Information Technology and Bionics, Pázmány Péter Catholic University, Budapest, Hungary. [3]János Szentágothai Doctoral School of Neurosciences, Semmelweis University, Budapest, Hungary. [4]Doctoral School of Psychology, Cognitive Sciences, Budapest University of Technology and Economics, Budapest, Hungary. [5]Faculty of Information Technology and Bionics, Pázmány Péter Catholic University, Budapest, Hungary. [6]Comparative Psychophysiology Research Group, Institute of Cognitive Neuroscience and Psychology, Research Center for Natural Sciences, Budapest, Hungary. [7]Department of Neurobiology, Weizmann Institute of Science, Rehovot, Israel. [8]Department of Anatomy and Histology, University of Veterinary Medicine, Budapest, Hungary. [9]These authors contributed equally: Boglárka Barsy, Kinga Kocsis.
✉e-mail: matyas.ferenc@ttk.mta.hu

signal monosynaptically and effectively to the LA and to a newly identified GABAergic amygdala population. By driving a complex intra-amygdala activity pattern, Calr$^+$LT cells play an instrumental role in the establishment of CS+US signals and the formation of fear memories in the LA. Furthermore, these thalamic cells alter their activity during memory trace formation and can discriminate between US-paired and unpaired signals during retrieval. Together, our study indicates that the LT pathway to the amygdala, composed of Calr$^+$LT neurons, provides associated and plastic signals for the acquisition of cue-related fear behavior.

Results

Calr$^+$LT cells project to the LA and are activated during fear learning. First, we identified which thalamic populations are connected to the LA. Thalamic cells retrogradely labeled from the LA with cholera toxin B subunit (CTB; Fig. 1a–c) were mainly located around the auditory thalamus (the MGN) in the PIL and the SG regions (Fig. 1b; Supplementary Fig. 1a–c). Since Calr$^+$ cells were specifically abundant in these lateral thalamic regions (Fig. 1b; Supplementary Fig. 1), we analyzed the Calr content of the CTB-labeled cells. The majority of them expressed Calr (Fig. 1c,d), which indicates that the thalamo–LA pathway is primarily formed by Calr$^+$ PIL and SG populations, hereafter collectively referred to as Calr$^+$LT neurons (Supplementary Information).

Next, we used an activity-dependent immediate early gene assay to investigate the involvement of the Calr$^+$LT neurons in transferring CS and/or US signals during fear learning (Fig. 1e; Supplementary Fig. 2). Expression of the immediate early gene *c-Fos* was analyzed in four groups of mice that received either a conditioning tone (7.5 kHz, 30 s; CS+) or a US (foot shock, 1 mA, 1 s; US), or a US-associated tone (CS+US). Naive mice were used as controls. While CS+ markedly increased c-Fos expression in the PIL and SG areas, US and CS+US further increased the number of activated neurons in the PIL region relative to what was observed in control mice (Fig. 1f–j; Supplementary Table 1). Since the majority of c-Fos-labeled cells were also Calr$^+$ (Fig. 1j; Supplementary Table 2), it was concluded that the LA can receive all relevant sensory information necessary for associative learning from Calr$^+$LT cells.

Calr$^+$LT cells transfer short-latency signals related to fear learning. The expression of c-Fos provided spatially precise data about the cellular origin of CS, US and CS+US information (Fig. 1) for the LA. However, it did not reveal whether these neurons can convey and integrate a CS and a US within a short time window[19] and supply the LA with a salient cue within 20 ms[7]. Thus, we performed extracellular in vivo recordings from Calr$^+$LT cells to investigate the time course of activation to short tone and footshock stimuli, as well as their possible potentiation to an associated footshock-coupled tone. *Calb2*-Cre mice (*Calb2* encodes Calr; Supplementary Fig. 1k–n) were injected with conditional Cre-dependent recombinant adeno-associated virus (AAV) expressing Channelrhodopsin 2 (ChR2); this model allowed us to optogenetically identify Calr$^+$LT cells in an orthodromic and amygdala-projecting cells (Calr$^+$LT→AMG) in an antidromic manner (Fig. 2a,b; $n=10$ mice; $N=60$ cells Calr$^+$; $N=42$ cells identified as Calr$^+$LT→AMG; $N=247$ non-tagged, putative Calr$^-$LT cells, including those located in the MGN). Single LT neurons showed activation to tone, footshock and/or tone+footshock signals with primarily short (5–50 ms; $N=32$ out of 37 tone-responsive cells; $N=61$ out of 85 footshock-responsive cells; $N=81$ out of 115 tone+footshock-responsive cells) but also with long (50–500 ms) (Fig. 2c–e; Supplementary Fig. 3; Supplementary Tables 3 and 4) latencies, indicating direct subcortical and broader network-involving sensory effects, respectively.

Significantly more Calr$^+$LT neurons were activated by foot shock and associative stimuli than Calr$^-$ cells (Fig. 2d). Furthermore, foot shock and footshock-associated tone stimuli activated significantly more Calr$^+$ cells (including Calr$^+$LT→AMG) than tone alone (Supplementary Tables 3 and 5), which is consistent with our c-Fos data (Fig. 1j). Multisensory enhancement was also present in the majority of Calr$^+$LT cells (18 out of 27), resulting in a larger short-latency activation to footshock-associated tone stimuli at the population level compared with unimodal tone or footshock cues (Fig. 2f,g). The majority of the enhanced cells (15 out of 18) did not show a unimodal response to tone, which suggests that auditory stimulation mostly evoked subthreshold activation in Calr$^+$LT neurons. Still, this could further potentiate the footshock signals. These data provide direct evidence to indicate that association of tone and foot shock can already take place at the level of the thalamus, before the amygdala. This associative signal drives the strongest short-latency activation (~17 ms on average) of Calr$^+$LT neurons, and this information is directly transferred to the amygdala.

The brainstem inputs to Calr$^+$LT neurons. Next, we investigated the possible upstream origins of the direct, short-latency cue-evoked signals to Calr$^+$LT cells using mono-trans-synaptic rabies tracing. To this end, we injected Cre-dependent helper virus and G-protein-deleted rabies virus (rabiesΔG) into the LT of *Calb2*-Cre mice (Fig. 3a–c). Calr$^+$LT neurons received major inputs from trans-synaptically labeled neurons in the inferior colliculus (IC) and the superior colliculus (SC) (Fig. 3d,f). The rabies-labeled neurons in the IC were preferentially located in the external and dorsal multisensory layers[24] and were sparsely distributed in primary auditory central regions (Fig. 3d). In the SC, the visual 'wide field' neurons in the superficial and the multisensory neurons in the intermediate and deep layers were similarly infected[25] (Fig. 3f). In addition, rabies-labeled cells were found in the PAG (Fig. 3e) and in the principal sensory trigeminal nucleus (Pr5) in lower quantities (Fig. 3g). Neurons in these locations can transfer monosynaptic and short-latency activation for auditory (IC), visual (SC) and nociceptive (SC, PAG and Pr5) cues[23,26] to the Calr$^+$LT cells.

To confirm the monosynaptic glutamatergic innervation of Calr$^+$LT neurons from the IC and the SC, we injected Cre-dependent enhanced yellow fluorescent protein (eYFP)-expressing AAV into the IC or SC of *vGlut2*-Cre mice (Fig. 3h,i,q,r). Transduced excitatory IC neurons (Fig. 3i) formed two types of synaptic connections in the LT[27] (Fig. 3j): large-sized axon terminals (~3–5 µm in diameter) were distributed in the Calr$^-$ MGN region (Fig. 3k,l), whereas small boutons (~1 µm) targeted the regions of Calr$^+$LT neurons (Fig. 3m–o). The existence of synaptic contact between the IC input and the Calr$^+$LT cells was confirmed by electron microscopy (Fig. 3p).

Glutamatergic SC neurons sent axon terminals exclusively to Calr$^+$LT territories (Fig. 3s,t) and formed asymmetrical synapses with Calr$^+$ elements (Fig. 3u–w). Altogether, these anatomical data provide further support that Calr$^+$LT cells integrate fast sensory and associated (tone+footshock) signals that originate from the brainstem and transfer these to the LA during fear conditioning.

Calr$^+$LT inputs target fear-learning-activated amygdala subnuclei. Next, we investigated the targets of Calr$^+$LT neurons in the amygdala. Using a novel viral strategy, we simultaneously transduced Calr$^+$ and Calr$^-$ populations in the LT of *Calb2*-Cre mice with a mixture of two AAVs. One transduced the Calr$^+$LT cells in a Cre-dependent manner with mCherry, while the other labeled only Cre$^-$ cells with eYFP (Fig. 4a). The majority of the lateral thalamic inputs in the LA was composed of mCherry-labeled Calr$^+$LT axons (~85%; Fig. 4b–d). Together with our retrograde tracing (CTB) data (Fig. 1), we concluded that Calr$^+$LT cells provide the major thalamic input to the LA. In addition, the centromedial (CeM) and the basomedial amygdala (BMA) also received Calr$^+$LT inputs (Supplementary Fig. 4a).

Just as selective activation of Calr$^+$LT cells was found during fear conditioning, an elevated c-Fos activation pattern was observed in the Calr$^+$LT-innervated amygdala regions, including

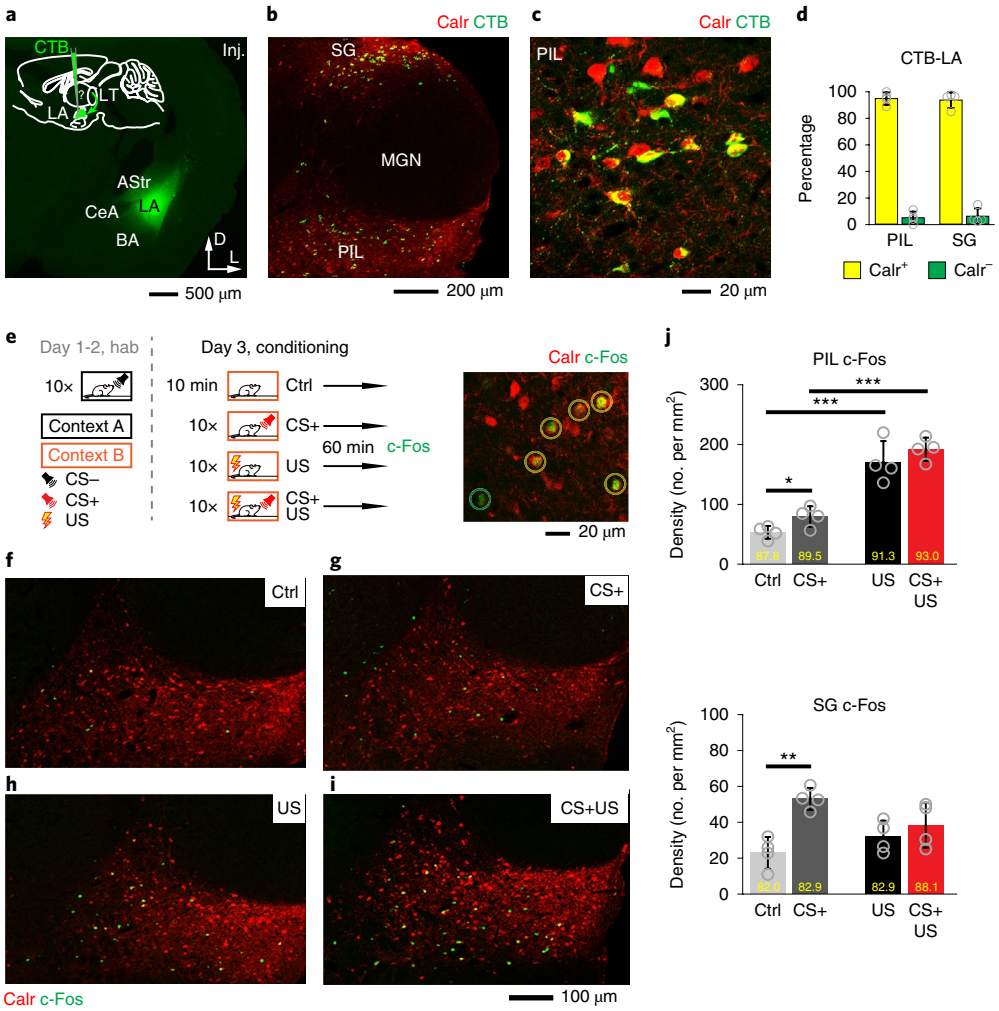

Fig. 1 | Calr⁺LT cells project to the LA and are activated by CS, US and US-associated CS stimuli. a, A retrograde tracer, CTB (green) injection (Inj.) site restricted to the LA. Inset: experimental design for identifying the source of thalamic inputs to the LA (green arrow and question mark). Arrows in the right corner indicate the dorsal (D) and lateral (L) orientation of the coronal section. **b**, Retrogradely labeled LA-projecting cells (CTB-LA) are dominantly present in the Calr-labeled (red) PIL and SG regions. Also see Supplementary Fig. 1. **c**, CTB-LA cells (green) expressing Calr⁺ in the PIL region. **d**, The majority of CTB-LA cells are Calr⁺ in both the PIL and SG nuclei ($n = 4$ mice; PIL + SG, $N_{CTB} = 180$, 572, 103 and 255 cells, $N_{Calr+CTB} = 167$, 563, 93 and 243 cells, Calr + CTB/all CTB, 94.2 ± 3.48% total). **e**, Left: schematic of the behavioral protocol using four groups of mice to identify the fear-conditioning-induced neuronal activation in the LT. Hab, habituation. Right: a high-magnification confocal image showing c-Fos activation (green) in the LT counterstained against Calr (red). Yellow circles highlight Calr⁺c-Fos⁺ double-labeled LT cells, while the green circle indicates a c-Fos⁺Calr⁻ cell. **f**–**i**, Representative images showing the density of c-Fos⁺ cells in a control (Ctrl), tone only (CS+), footshock only (US) and CS + US cases. **j**, c-Fos density in the PIL and SG regions. Open circles indicate individual mouse data;, yellow numbers in the graphs represent the proportion of Calr⁺c-Fos⁺ cells. Data in **d** and **j** are shown as the mean ± s.d.; two-sided *t*-test. Images in **a**–**c** and **e**–**i** are representative of $n = 4$ mice. See also Supplementary Tables 1 and 2 for further data and Supplementary Table 5 for statistical details. $^*P < 0.05$; $^{**}P < 0.01$; $^{***}P < 0.001$.

the LA, the CeM and the BMA (Fig. 4e–i; Supplementary Fig. 4b; Supplementary Table 6a,b). Notably, the strongest c-Fos activation was found in a previously unspecified region dorsal to the dorsomedial intercalated cell mass of the amygdala (dmITC) (indicated by yellow arrows in Fig. 4g,h). Neurons in this region, hereby named supra-intercalated cluster of neurons (SIC), also received Calr⁺LT input (Fig. 4j). However, the majority of these cells did not express either mGluR1α or FoxP2 (Fig. 4k,l), which are characteristic of the noxious-stimulus-activated ITC[28]. To identify their neurotransmitter profile, we transduced all GABAergic neurons in this region with a Cre-dependent eYFP-encoding AAV in *vGat*-Cre mice. After recovery, mice were exposed to foot shock (US) (Fig. 4m), which greatly increased c-Fos expression in SIC (Fig. 4n). The majority of the c-Fos⁺ cells were co-labeled with YFP (Fig. 4n,o), which suggests that a previously unidentified GABAergic population in the amygdala, the SIC, dominates in noxious sensory processes via Calr⁺LT inputs (Fig. 4p).

Calr⁺LT inputs strongly shape the activity of LA and SIC neurons. To test the functional impact of Calr⁺LT innervation on the LA and the SIC, we transduced Calr⁺LT neurons with a Cre-dependent halorhodopsin (NpHR3.0)-expressing AAV and performed in vivo extracellular recordings from the amygdala (Fig. 5a; see Methods). Optogenetic inhibition of Calr⁺LT→AMG axons significantly decreased or increased the spontaneous firing of a subset of neurons. These modulations were present among both the principal and putative GABAergic neurons of the LA as well as the SIC (Supplementary Fig. 5a–e), which demonstrates that there are Calr⁺LT-driven feedforward excitatory and inhibitory mechanisms in the LT–amygdala pathway. In addition, we investigated the

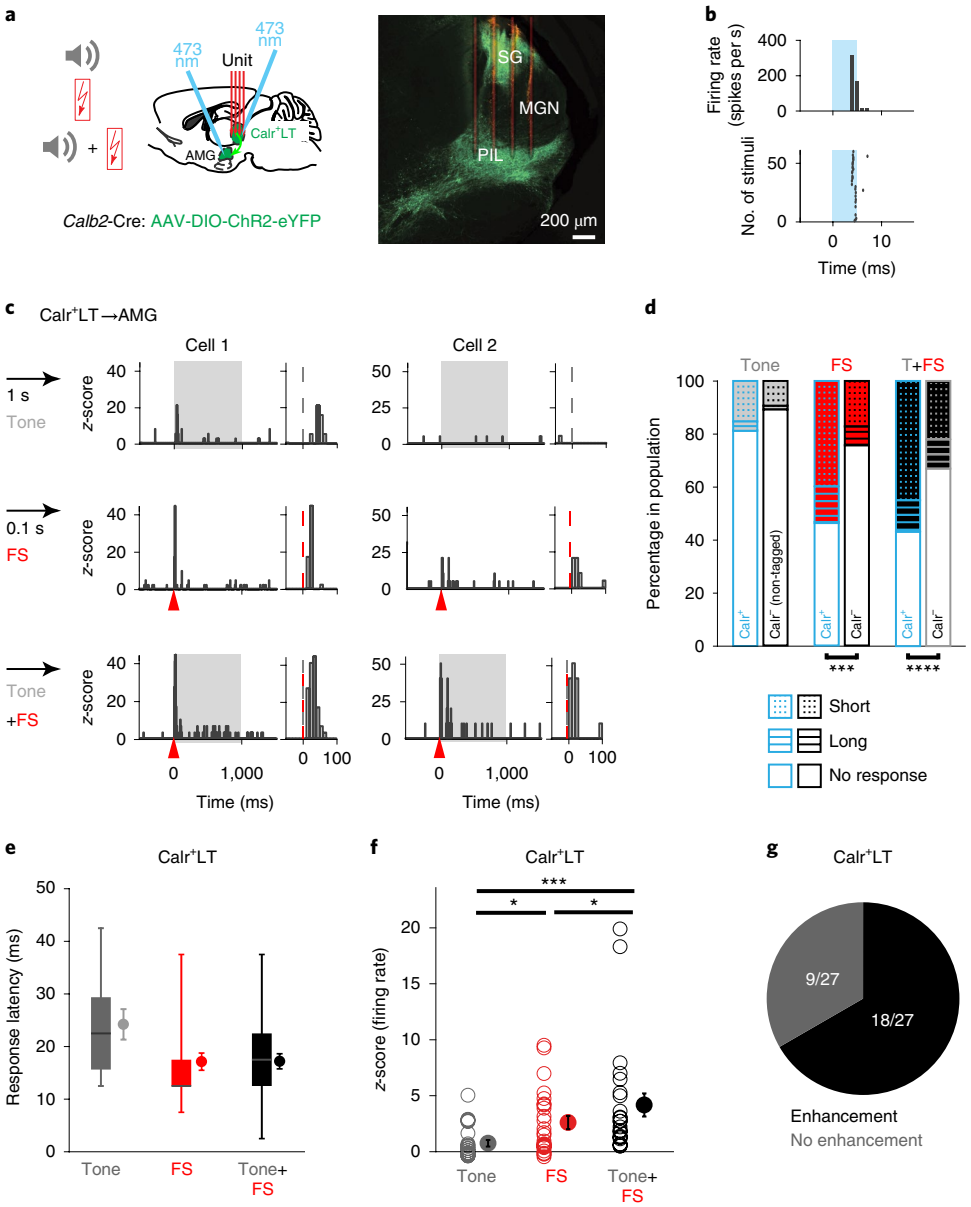

Fig. 2 | Selective and fast aversive cue-associated sensory signaling by Calr⁺LT cells. a, Left: schematic of in vivo unit recordings from LT cells with delivery of tone, footshock and paired tone + footshock signals ($n = 10$ mice). Right: a coronal section of a LT with AAV-DIO-ChR2-infected Calr⁺ cells (green) and showing the trajectory of the four-shank silicon probe (red). **b**, Antidromic optogenetic tagging (blue) of a Calr⁺LT→AMG cell in the PIL. **c**, A Calr⁺LT→AMG cell (Cell 1) showing short-latency tone (gray), footshock (FS; red arrowheads) and enhanced associative tone + footshock activations. Another Calr⁺LT→AMG cell (cell 2) with enhanced tone + footshock activation without tone-alone response. Right: zoom-in of traces on the left highlighting the time-course of the evoked responses. Bin size, 10 ms. **d**, Graphs showing the relative proportions (percentage) of short-latency-evoked and long-latency-evoked responses within the Calr⁺LT→AMG, total Calr⁺LT and non-tagged LT cell populations. χ^2 test. **e**, Population data for the estimated latencies for short-latency tone, footshock and associative tone+footshock-evoked activation of Calr⁺LT cells within a 5–50 ms post-stimulus time window. Horizontal lines in box plots indicate medians, box limits indicate first and third quartiles, and vertical whisker lines indicate minimum and maximum values. Filled circles represent the mean ± s.e.m. **f**, Population data for average *z*-score of firing rate as the result of sensory stimuli in the case of Calr⁺LT neurons with short-latency (<50 ms) tone + footshock responses ($N = 27$ cells). Mean ± s.e.m. Friedman ANOVA with Wilcoxon matched-pairs test (two-sided). **g**, Proportion of multisensory enhancement (augmented tone+footshock signal) in the same cells as in **f**. $^{***}P < 0.001$; $^{****}P < 0.0001$. All results from the in vivo acute thalamic electrophysiology data analysis are summarized in Supplementary Tables 3 and 4; details of statistical analyses are provided in Supplementary Table 5.

contribution of Calr⁺LT cells to the sensory activation of amygdala neurons. Similar to Calr⁺LT neurons, more LA cells and SIC were activated by foot shock and footshock-associated tone than to tone alone[29] (Fig. 5b–d; Supplementary Fig. 5h; Supplementary Table 7). Within the LA, more interneurons than principal cells were activated by the CS+US signal (Fig. 5e; Supplementary Fig. 5f–h; Supplementary Table 7). Most of them exhibited short-latency responses (~20 ms on average; Supplementary Fig. 5g; Supplementary Table 4). The time course of evoked responses in Calr⁺LT cells and the amygdala (2–3 ms difference in latency) also suggested that short-latency amygdala activation is derived directly from the Calr⁺LT cells. Indeed, optogenetic silencing

of Calr$^+$LT→AMG axons significantly affected the responses of LA neurons and SIC evoked by tone, foot shock or associated tone+footshock (Fig. 5b–e; Supplementary Fig. 5h; Supplementary Table 7). In addition to the inhibited responses, many LA neurons and SIC enhanced their evoked activation (Fig. 5e; Supplementary Fig. 5f). Furthermore, some neurons only showed activation to sensory stimuli during Calr$^+$LT→AMG optogenetic silencing, which also indicated the presence of a strong thalamic-driven disinhibitory mechanism in the amygdala (Fig. 5e; Supplementary Fig. 5h; Supplementary Table 7).

There are multiple candidates for executing these inhibitory and disinhibitory actions in the amygdala. Since SIC send axon collaterals to other SIC as well as to LA cells (Fig. 5f–i), this population could be equally involved in the feedforward inhibitory and disinhibitory thalamic effects, similar to the ITC and local LA interneurons[30–33] (Fig. 5c–e; Supplementary Fig. 5f,h). These results demonstrate that multimodal and associated signals carried by Calr$^+$LT inputs can control the activity patterns of the amygdala in a complex manner: directly via feedforward excitation and feedforward inhibition as well as indirectly through the disinhibition of principal neurons via the activation of SIC and local interneurons (Fig. 5j).

The Calr$^+$LT→AMG pathway is essential for fear learning. Next, we examined the behavioral effects of the Calr$^+$LT→AMG pathway with optogenetic axonal silencing. *Calb2*-Cre mice were bilaterally injected in the LT with Cre-dependent AAV-DIO-NpHR-eYFP or AAV-DIO-eYFP (as control) and implanted with optic fibers above the amygdala (Fig. 6a–c; Supplementary Fig. 6a). Green light (532 nm) illumination of Calr$^+$LT→AMG axons had no effect on spontaneous behavior in a novel environment (open field; Supplementary Fig. 6b). Next, we tested the effects of this optogenetic manipulation on behavior during a discriminative fear-conditioning paradigm. Mice were habituated to the non-conditioned tone (CS–, white noise) for 2 days. On day 3, the conditioned tone (CS+, 7.5 kHz) was terminated with foot shock (US) and paired with optogenetic silencing (for the entire period of the 30 s of CS+). This conditioning protocol developed acute freezing behavior in control animals (YFP), but resulted in a significantly lower freezing level in NpHR mice (Fig. 6d; Supplementary Video 1). As our intervention kept most pain pathways intact[34], the observed difference in the level of freezing behavior between YFP and NpHR mice can be better explained by an impairment in fear learning than by a disruption of nociceptive signaling because of the presence of footshock-induced escape behavior (jumping; Supplementary Video 1) and vocalizations (Supplementary Fig. 6d). On day 4, in cued fear-memory retrieval, CS– and CS+ presentations evoked decreased levels of freezing in the NpHR mice relative to the YFP group (Fig. 6e; Supplementary Video 2), and this effect was accompanied by a lack of cue discrimination. On day 5, contextual freezing was also lower in NpHR mice (Fig. 6f). The greatly reduced freezing behavior during the retrieval days (days 4 and 5) suggests that there is a deficit in fear memory linked to the conditioning environment (cue and context).

Cued and contextual freezing behavior of the NpHR mice was indistinguishable from those of the non-shocked YFP animals, which only received the CS during the conditioning phase (CS-only YFP group). To test whether the NpHR animals had a similar behavioral phenotype to the CS-only YFP animals, on day 8, we placed the animals in a novel stressful situation on an elevated plus-maze (EPM) apparatus. The EPM assay allowed us to simultaneously monitor anxiety level and risk assessment. Five days after conditioning, the NpHR mice showed a similar ratio of closed-arm versus open-arm time and total-arm entries to the non-shocked mice (Supplementary Fig. 6e). Risk assessment (as indicated by the animal exhibiting the defensive stretch–attend posture) and grooming behavior of NpHR mice were also comparable to the CS-only YFP mice, but significantly different from the YFP group (Fig. 6g,h). These data collectively show that the general aversive state of NpHR mice was similar to the non-shocked controls, and suggest that optogenetic silencing of Calr$^+$LT→AMG input prevented both short-term and long-term behavioral consequences of fear acquisition.

In a separate group of animals, short optogenetic silencing of the Calr$^+$LT→AMG axons, only during the last 5 s of CS+ presentation, including the US, resulted in similar behavioral changes as silencing the entire 30-s conditioning phase (Supplementary Fig. 6f–j). This shows that preventing the associative CS+US information flow alone was sufficient to disrupt fear memory processes.

In addition to the impaired contextual fear response in NpHR mice (Fig. 6f), inhibition of Calr$^+$LT→AMG axons during contextual fear retrieval in a separate cohort of mice decreased contextual freezing behavior (Supplementary Fig. 6k–m). This indicates that Calr$^+$LT neurons also transfer visual and multisensory information arising from collicular inputs (Fig. 3), which may contribute to contextual coding in affective behavior. Thus, information carried by the Calr$^+$LT→AMG pathway during fear conditioning is essential for the development of adaptive cued and contextual fear memory.

Fear-learning-induced plasticity in Calr$^+$LT→AMG neurons. Thalamic cells spatially matching Calr$^+$LT neurons can undergo plasticity as a result of fear conditioning[5,21]. To clarify whether the activity of Calr$^+$LT cells shows experience dependency in auditory fear learning, we analyzed their immediate early gene expression

Fig. 3 | Monosynaptic brainstem inputs to Calr$^+$LT neurons. a, Experimental design for rabies-mediated trans-synaptic tracing from Calr$^+$LT cells. **b**, Example confocal image illustrating AAV-FLEX-TVA-eGFP-oG (helper) and rabies(ΔG)-EnvA-mCherry-labeled (rabies) cells in the PIL and the SG nuclei after injections depicted in **a**. **c**, High-magnification confocal images showing rabies-labeled (red) and helper-labeled (green) neurons in the PIL. Starter cells transduced by both the helper and rabies viruses are outlined with a dashed line. Asterisks indicate double-negative cells. **d**–**g**, Example confocal images showing rabies(ΔG)-mCherry-labeled cells in the IC (dorsal, external and central (DIC, EIC and CIC, respectively); **d**), in the PAG (**e**), in the SC (superficial, intermediate and deep (sSC, iSC and dSC, respectively) layers; **f**) and in the Pr5 (**g**). Aq, aqueduct; 7n, facial nerve. **h**, Schematic drawing for AAV-DIO-eYFP injections into the IC of *vGlut2*-Cre mice. **i**, Image of a representative injection site in the IC. **j**, IC inputs (YFP, green) to LT co-stained for Calr (red). White framed areas for the MGN are enlarged in **k** and **l** and for the PIL in **m**–**o**. **k**,**l**, A representative high-magnification *Z*-stack confocal image (7 µm total in depth) from the MGN (Calr$^-$; **k**) illustrating large-sized IC axon terminals (white arrowheads; **l**). **m**–**o**, A representative high-magnification *Z*-stack confocal image (7 µm total in depth) from PIL (**m**; co-stained for Calr shown in **n**) illustrating small-sized IC axon terminals (white arrowheads; **o**) in close apposition with the Calr$^+$ PIL cells (**o**). **p**, An electron micrograph showing an immunogold-labeled Calr$^+$ dendrite (d_{Calr^+}; covered by small black particles, area shaded with pink) in the PIL receiving an asymmetrical synaptic contact (black arrowhead) from a DAB-labeled (diffuse black precipitate) vGluT2$^+$ IC axon terminal (IC_{vGluT2^+}; shaded green). **q**, Schematic for AAV-DIO-eYFP injections into the SC of *vGlut2*-Cre mice. **r**, Image of a representative injection site in the SC targeting the sSC and the iSC. **s**, SC inputs (YFP, green) to the LT co-stained for Calr (red). **t**, A representative high-magnification *Z*-stack confocal image (7 µm total in depth) with vGluT2$^+$ SC axon terminals (white arrowheads) in close proximity to Calr$^+$ PIL neurons (red). **u**–**w**, Electron micrographs showing immunogold-labeled Calr$^+$ dendrites (d_{Calr^+}; **u**,**v**) and a spine (sp_{Calr^+}; **w**) in the PIL receiving asymmetrical synaptic contacts (black arrowheads) from DAB-labeled, vGluT2$^+$ SC axon terminals (SC_{vGluT2^+}). A non-stained axon terminal outlined with a dashed line (**u**) also gives synaptic input onto the Calr$^+$ dendrite. Images in **b**–**g**, **i**–**p** and **r**–**w** are representative of $n = 3$ mice.

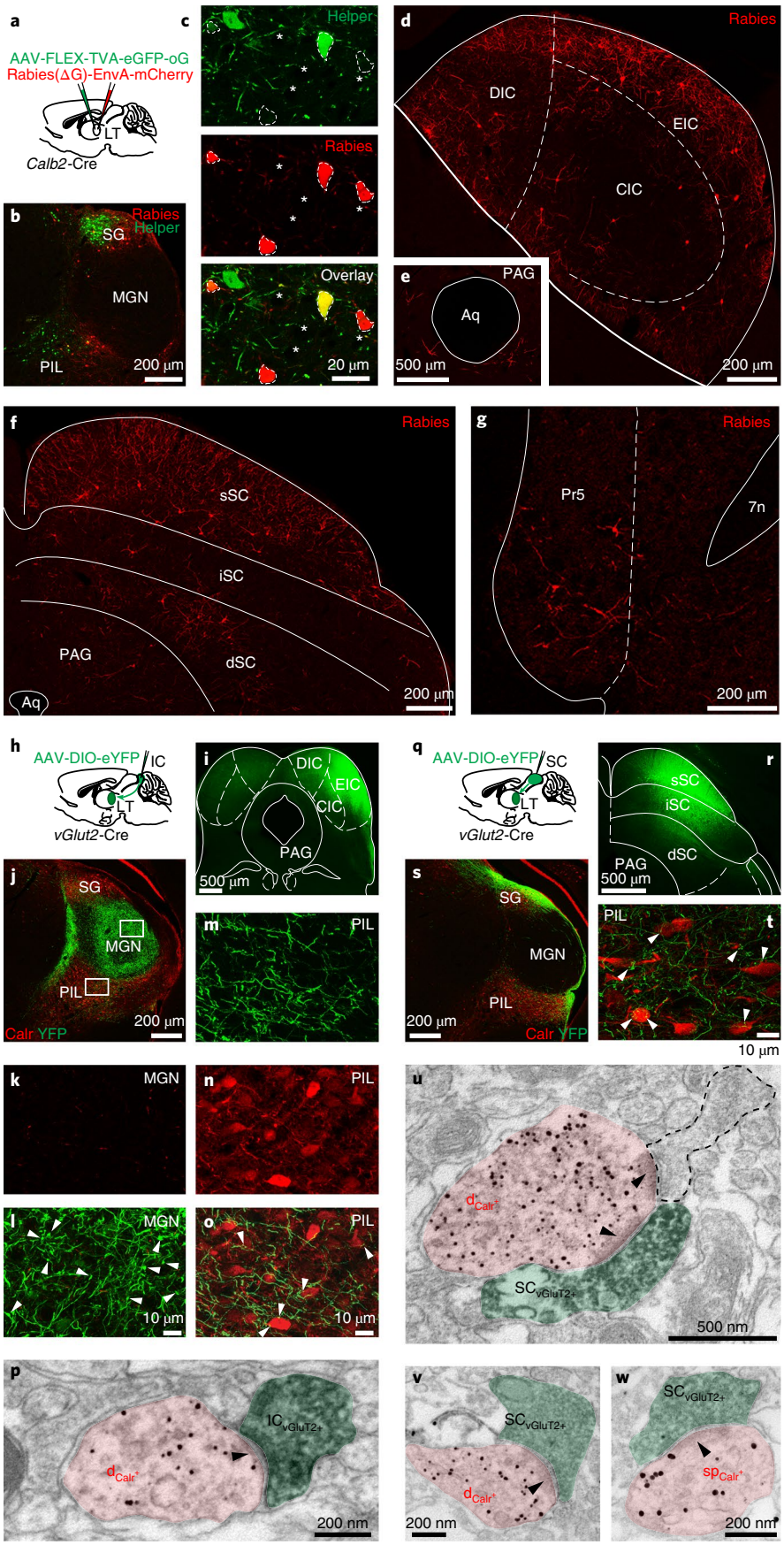
a
AAV-FLEX-TVA-eGFP-oG
Rabies(ΔG)-EnvA-mCherry
LT
Calb2-Cre
b
Rabies
Helper
SG
MGN
PIL
200 μm
c
Helper
Rabies
Overlay
20 μm
d
Rabies
DIC
EIC
CIC
200 μm
e
PAG
Aq
500 μm
f
Rabies
sSC
iSC
PAG
dSC
Aq
200 μm
g
Rabies
Pr5
7n
200 μm
h
AAV-DIO-eYFP
IC
LT
vGlut2-Cre
i
DIC
EIC
CIC
PAG
500 μm
j
SG
MGN
PIL
Calr YFP
200 μm
k
MGN
l
MGN
10 μm
m
PIL
n
PIL
o
PIL
10 μm
q
AAV-DIO-eYFP
SC
LT
vGlut2-Cre
r
sSC
iSC
dSC
PAG
500 μm
s
SG
MGN
PIL
200 μm
Calr YFP
t
PIL
10 μm
u
dCalr+
SCvGluT2+
500 nm
p
ICvGluT2+
dCalr+
200 nm
v
SCvGluT2+
dCalr+
200 nm
w
SCvGluT2+
spCalr+
200 nm

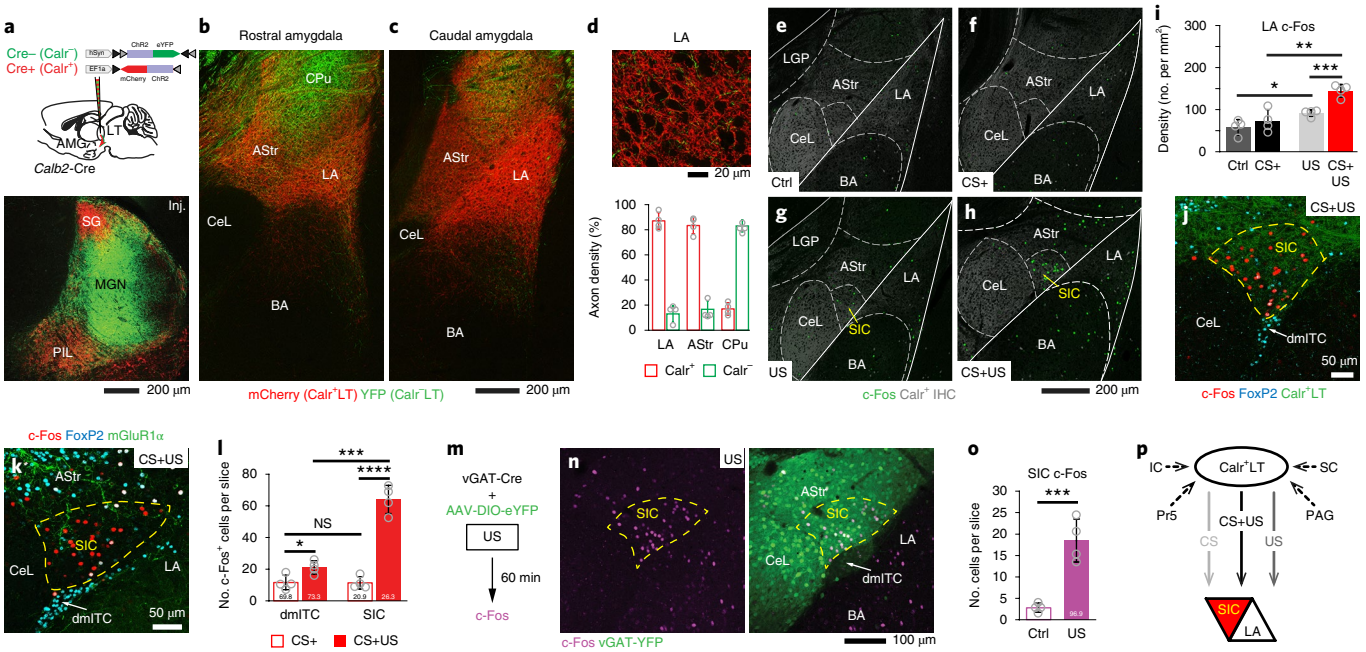

Fig. 4 | Calr$^+$LT neurons target the fear-conditioning-activated LA neurons and SIC. a, Top: schematic of selective viral labeling of Calr$^+$LT (red) and Calr$^-$LT cells (green). Bottom: image of the injection site in the LT. **b,c**, Coronal sections from two rostrocaudal planes showing distinct Calr$^+$LT (mCherry, red) and Calr$^-$LT (YFP, green) innervation of the amygdala with subnuclear specificity. See also Supplementary Fig. 4. **d**, Top: high-magnification confocal image taken from the LA. Bottom: quantification of LT axonal lengths in the LA, the AStr and the neighboring striatal region (CPu) (see also Methods). **e–h**, Confocal images showing amygdala subnucleus-specific c-Fos activation (green) in a control (Ctrl; **e**), tone only (CS+; **f**), footshock only (US; **g**) and CS+US animal (**h**) during fear conditioning. This was the same experiment as in Fig. 1 (see also Supplementary Fig. 2 and Supplementary Table 6a,b). Immunohistochemical staining against Calr (Calr$^+$ IHC; gray) was used to outline different amygdala subregions (see also Supplementary Fig. 4a). CeL, lateral part of the CeA; LGP, lateral globus pallidus. **i**, Population data for c-Fos activation in the LA ($n = 4$ mice each). **j**, High-magnification confocal image from a CS + US mouse with the highest c-Fos density (red) in the SIC, which is innervated by Calr$^+$LT→AMG axons (green). **k**, c-Fos activated cells (red) in the SIC are distinct from FoxP2 (cyan) or mGluR1α-expressing (green) dmITC neurons. **l**, Population data for the density of c-Fos$^+$ cells in the SIC and the dmITC ($n = 4$ mice for each region). Numbers at the bottom of each bar indicate the proportion of FoxP2$^+$ cells within the c-Fos-labeled dmITC and SIC. **m**, Experimental design to test the GABAergic nature of footshock (US)-activated SIC neurons. **n**, A confocal image showing US-evoked c-Fos activation (magenta, left) and the YFP transduced vGAT (green) neurons in the SIC. **o**, Grouped data for the density of US-activated c-Fos$^+$ cells compared with control mice, and their colocalization with vGAT-YFP labeling in SIC ($n_{c\text{-}Fos} = 659$ cells, $n_{c\text{-}Fos+vGAT} = 638$, $n = 4$ mice; vGAT$^+$/all c-Fos: 96.90 ± 1.1%). **p**, Summary diagram based on Figs. 1–4 showing that Calr$^+$LT input carries CS, US and CS + US signals originating from the brainstem and transfers them to the LA and SIC. Arrows with darker colors indicate stronger signals. Confocal images in **a–d**, **e–h**, **j**, **k** and **n** are representative of $n = 4$ mice. Data in **d**, **i**, **l** and **o** represent the mean ± s.d; $^*P < 0.05$; $^{**}P < 0.01$; $^{***}P < 0.001$; $^{****}P < 0.0001$ (two-sided t-test). See Supplementary Table 5 for statistical details.

(see Methods) after the cued fear-retrieval phase. Two groups of mice were used in the conditioning phase: one group received CS+US and the other group received CS+ only (CS only). During cued fear retrieval, mice in both groups were presented with either CS– or CS+. The retrieval phase was omitted in a third group of CS+US mice (pre-Retr. group) to set the baseline of c-Fos expression 24 h after fear conditioning (Fig. 7a). Tone-induced discriminative fear behavior was retrieved in CS+US mice, since presentation of CS+ but not CS– resulted in elevated freezing levels. CS-only animals showed no fear to either of the auditory cues (Supplementary Fig. 7a). Next, we quantified the auditory-signal-evoked c-Fos expression in the LT (Fig. 7a–f; Supplementary Tables 1 and 2). CS+ increased while CS– decreased the number of c-Fos$^+$ neurons in the Calr$^+$LT region of the CS+US mice compared with the CS-only mice (Fig. 7c–f), which suggests that cue sensitivity of the Calr$^+$LT cell population underwent plasticity that is tightly related to the behavioral outcome.

To test the presence of learning-induced plasticity in individual Calr$^+$LT→AMG cells, we acquired single-unit data ($N = 18$) from chronically implanted mice throughout the 3-day-long fear-learning paradigm (Fig. 7g). Retrogradely labeled Calr$^+$LT→AMG cells were optogenetically identified, and their evoked responses to auditory stimuli were monitored before fear conditioning and during cued fear retrieval (Fig. 7h–l; Supplementary Fig. 8). Activity of 9 out of 18 thalamic cells showed modulation in parallel with the formation of cued memory (Fig. 7k,l; Supplementary Fig. 8e,f). Fear learning prominently increased the activation of Calr$^+$LT→AMG neurons to CS+ (before conditioning, Pre-Cond. CS+, $N = 1$ cell versus after conditioning, Retr. CS+, $N = 5$ cells). In addition, 6 out of 18 cells showed discriminative activity pattern during retrieval. Together, our anatomical and electrophysiological findings indicate that the Calr$^+$LT→AMG pathway not only transfers associated signals during fear conditioning but also its activity shows plasticity as a result of fear memory formation.

The fear-learning-induced changes in the Calr$^+$LT population could be responsible for the long-term modulation of amygdala circuits[29,33]. Similar to the c-Fos activation pattern found in fear conditioning, fear retrieval primarily activated the Calr$^+$LT-cell-innervated LA and SIC, as well as the CeM and BMA (Supplementary Fig. 7b; Supplementary Table 6a,b). Interestingly, c-Fos activation induced by CS– and CS+ was similar in all amygdala regions, which is in agreement with recent c-Fos[35] and imaging data[29]. This observation suggests that it is not the size of the amygdala population but its thalamic input characteristics that shape behavioral outcomes.

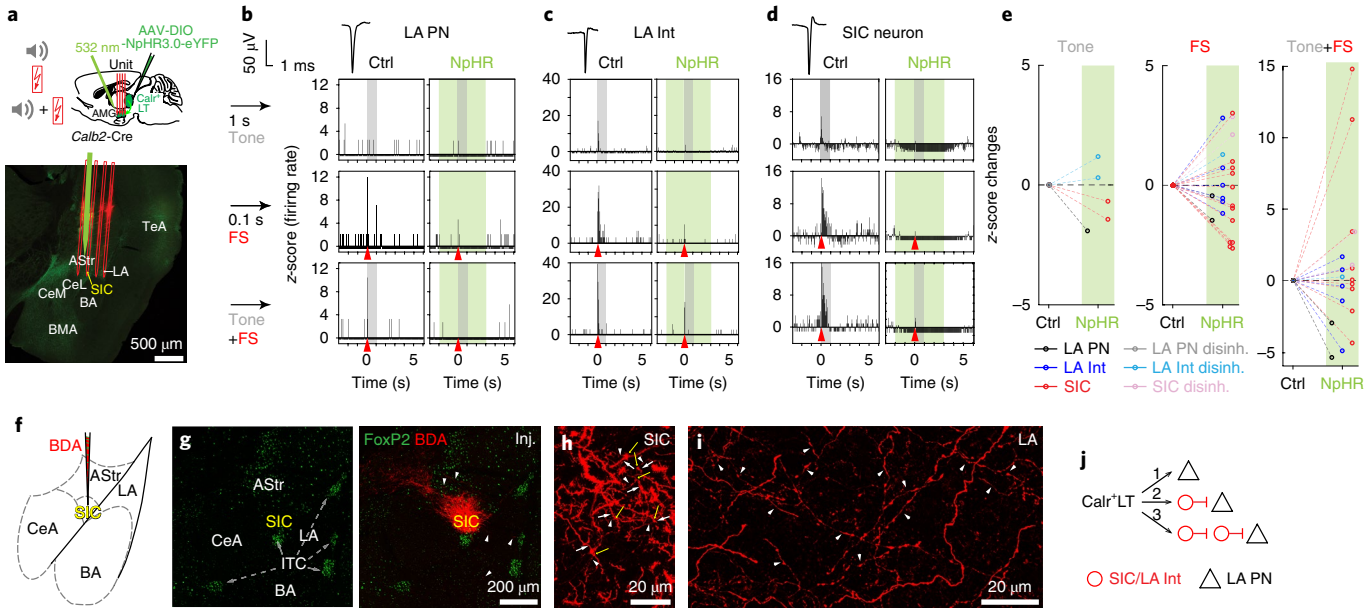

Fig. 5 | Calr⁺LT neurons control the multisensory activation of amygdala cells in a complex manner. a, Top: schematic of optogenetic inhibition of NpHR-labeled Calr⁺LT→AMG inputs and unit recordings in the amygdala. Bottom: a representative coronal section indicating the insertion tracks of the optic fiber (blue) and a four-shank electrode (red) in the amygdala. **b**–**d**, Optogenetic inhibition (green) of NpHR⁺ Calr⁺LT inputs alters sensory-evoked amygdala activity compared to the control condition ($n = 11$ mice). Evoked sensory responses of a LA principal cell (LA PN; **b**), a LA interneuron (LA Int; **c**) and a neuron from the SIC (SIC neuron; **d**) are inhibited by NpHR-mediated Calr⁺LT axonal inhibition. Gray shadings represent the delivery of tone, red arrowheads mark the delivery of footshock stimuli. **e**, Pooled data for average *z*-scored activity changes (<50 ms) elicited by optogenetic Calr⁺LT→AMG axonal silencing (green shaded area) during different sensory stimulation. 'Disinh' indicates cells without evoked response during control condition but with activation (disinhibition) as a result of Calr⁺LT axonal inhibition. All results from in vivo acute amygdala electrophysiology data analysis are summarized in Supplementary Table 7; details of statistical analyses are provided in Supplementary Table 5. **f**, Schematic of BDA injections into the SIC. **g**, BDA (red; right) injection site in the SIC outside the FoxP2-labeled ITC (green; left and right). Arrowheads (right) point to BDA-labeled axons (red) in the LA and the AStr. **h**, BDA-labeled cells within the SIC form local axon collaterals (white arrowheads), which are positioned in close proximity (yellow arrows) to BDA-labeled dendrites (white arrows). **i**, BDA-labeled axon terminals in the LA (white arrowheads). Confocal images in **g**–**i** are representative of $n = 4$ mice. **j**, Summary drawing indicating the complex activity patterns of LA PN and LA Int/SIC neurons elicited by excitatory Calr⁺LT inputs: (1) feedforward excitation; (2) feedforward inhibition via local LA Int or SIC; and (3) LA Int/SIC-mediated disinhibition.

The Calr⁺LT→AMG route is necessary for the retrieval of cued fear memory. Finally, we assessed whether activity of the Calr⁺LT→AMG route, changed by fear learning, is necessary for the retrieval of conditioned fear memory. After successful and similar fear learning in YFP and NpHR mice during the conditioning phase, we optogenetically inhibited the Calr⁺LT→AMG axons during CS+ presentations in retrieval (Fig. 8a–c). NpHR mice showed decreased freezing induced by CS+ compared with controls (YFP); thus, the NpHR mice had impaired memory retrieval (Fig. 8d).

These changes were temporary and restricted to the conditioned cue-induced behavior, as NpHR animals showed similar contextual fear responses (Fig. 8e), risk assessment and grooming behavior to the YFP mice (Fig. 8f,g). These data show that, as fear acquisition was intact, optogenetic manipulation during cued fear retrieval only blocked the Calr⁺LT→AMG information flow necessary for ongoing signal discrimination but did not abolish other features—for example, the contextual aspect—of the consolidated fear memory.

Calr⁺LT cells equally control cortical and basal ganglia circuitry in associative behavior. Besides the amygdala projection, hypothalamic and temporal cortical regions are innervated by both Calr⁺LT and Calr⁻LT populations, but in a distinct pattern (Supplementary Fig. 9a–f). While the Calr⁻ cells were preferentially connected to sensory cortical areas (primary auditory cortex (Au1) and ventral secondary auditory cortex (AuV)), Calr⁺LT neurons targeted the AuV and the temporal association cortex (TeA), as well as the insular cortices. The latter cortical regions provide the main cortico–LA projection (Supplementary Fig. 9g–q) and are involved in long-term fear memory storage and retrieval[36]. We further found that ~40–60% of Calr⁺LT cells targeted both the cortex and the LA (Supplementary Fig. 9r–w). This indicates that the same Calr⁺LT population has a dual thalamic influence on the LA in fear learning and memory recall: directly via the thalamo–amygdala route and indirectly via the thalamo–cortico–amygdala route[1] (Supplementary Fig. 9q).

In addition, Calr⁺LT cells sent axonal projections to the amygdalostriatal transition area (AStr), which is suggested to participate in sensory processes during fear learning[8] (Supplementary Fig. 10). The majority of the AStr-projecting LT neurons were also Calr⁺ and distributed similarly to those projecting to the LA (Supplementary Fig. 10a–g). Double retrograde labeling with injections of A488-conjugated and A555-conjugated CTB into the LA and AStr (Supplementary Fig. 10h–k) showed that a substantial proportion (20–30%) of LT cells projected to both regions (Supplementary Fig. 10l,m). This suggests that the Calr⁺LT cell population can synchronously shape the activity of the amygdala and AStr neurons in fear behavior. In accordance with this, fear conditioning and cued fear-retrieval-evoked c-Fos activation patterns were comparable between the AStr and the LA (Supplementary Fig. 10n,o; Supplementary Table 6a,b), which is potentially as a result of Calr⁺LT neuron activity. Actually, both the spontaneous (Supplementary Fig. 10p,q) and the sensory-evoked firing rate of the recorded AStr cells (Supplementary Fig. 10r; Supplementary Tables 6a,b and 7)

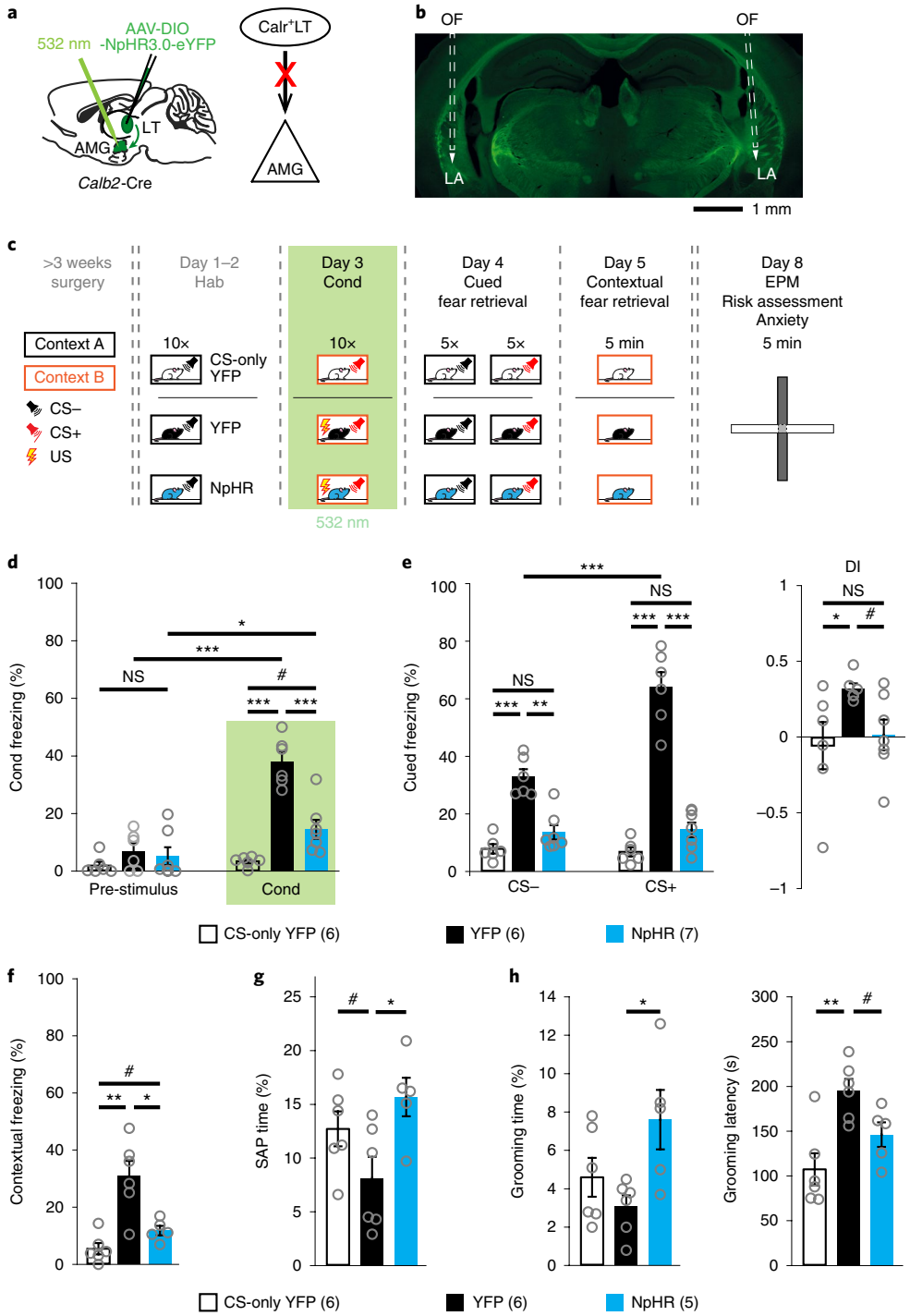

Fig. 6 | Calr^{+}LT→AMG inputs shape fear learning. a, Left: schematic of viral injections and optic fiber implantation above the amygdala. Right: experimental design for axonal inhibition of Calr^{+}LT inputs in the amygdala. **b**, An example coronal section with bilaterally implanted optic fibers (OFs). **c**, Schematic of the protocol used for investigating the behavioral impact of optogenetic silencing of Calr^{+}LT→AMG inputs (green shading) during auditory fear-conditioning (day 3). **d**, Freezing behavior during fear conditioning (Cond.). Repeated-measures ANOVA for group by time interactions ($F_{2,16} = 36.9894$, $P = 1 \times 10^{-6}$) with unequal *N* honest significant difference (HSD) test. **e**, Left: freezing behavior during the cued fear-memory retrieval. Repeated measures ANOVA for group by time interactions ($F_{2,16} = 29.5351$, $P = 4 \times 10^{-6}$) with unequal *N* HSD test. Right: the calculated DI values. Kruskal–Wallis ANOVA ($H_{2,19} = 5.7301$, $P = 0.057$) with Mann–Whitney *U*-test (two-sided). **f**, Freezing behavior in contextual fear retrieval. Kruskal–Wallis ANOVA ($H_{2,17} = 10.1036$, $P = 0.0064$) with Mann–Whitney *U*-test (two-sided). **g**, Risk assessment behavior measured from time spent in the stretch-attend posture (SAP) in the EPM test environment. Kruskal–Wallis ANOVA ($H_{2,17} = 6.6121$, $P = 0.0459$) with Mann–Whitney *U*-test (two-sided). **h**, Grooming behavior. Left: time spent by grooming in the EPM. Kruskal–Wallis ANOVA ($H_{2,17} = 5.5473$, $P = 0.0624$) with Mann–Whitney *U*-test (two-sided). Right: grooming latency. Kruskal–Wallis ANOVA ($H_{2,17} = 8.8810$, $P = 0.0118$) with Mann–Whitney *U*-test (two-sided). For **d**–**h**, data show the mean ± s.e.m; the number of mice are in parentheses next to the keys for the charts. $0.05 > {}^{\#}P < 0.1$, $^{*}P < 0.05$, $^{**}P < 0.01$, $^{***}P < 0.001$. See Supplementary Table 5 for statistical details.

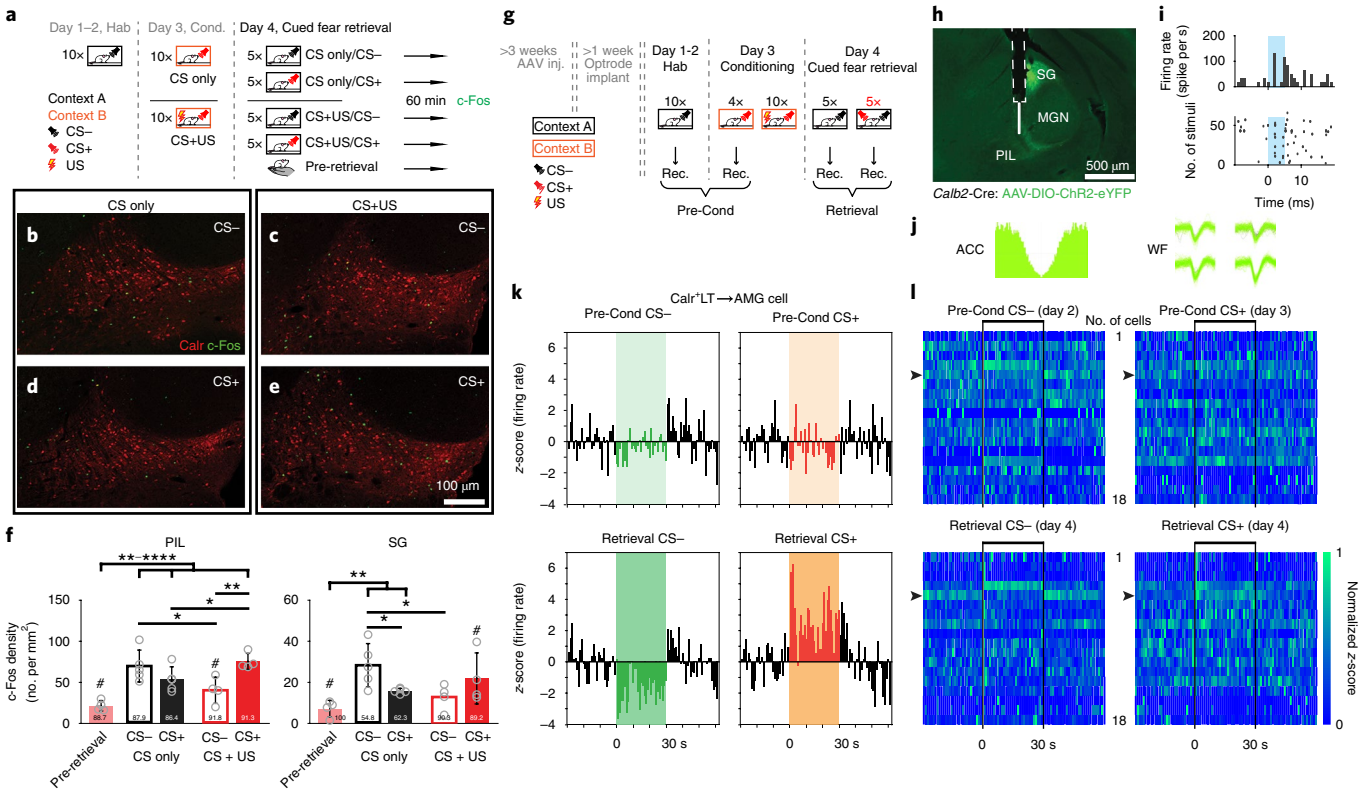

Fig. 7 | Fear learning induces changes in the activity pattern of Calr⁺LT neurons. a, Schematic design for measuring cued fear-retrieval-induced c-Fos activation. **b**–**e**, Representative confocal images indicating c-Fos activation (green) in PIL upon presentation of non-conditioned (CS–; **b**,**c**) and conditioned (CS+; **d**,**e**) auditory signals to CS-only (**b**,**d**) and CS + US (**d**,**e**) animals (see Methods). **f**, Density and proportion of PIL and SG c-Fos⁺ cells. Open circles indicate individual mouse data, numbers inside the bars represent the proportion of Calr⁺c-Fos⁺ cells. Data represent the mean ± s.d; two-sided *t*-test. $n_{\text{Pre-retrieval}} = 4$, $n_{\text{CS+US}} = 4$, $n_{\text{CS only}} = 5$ mice (**a**–**f**). See also Supplementary Tables 1 and 2 for quantitative data, and Supplementary Table 5 for statistical details. **g**, Experimental design for optrode recordings (rec.) of Calr⁺LT→AMG neuronal activity in freely moving mice during fear learning (days 2–4; $n = 10$ mice, $N = 18$ cells). **h**, A coronal section showing retrogradely labeled Calr⁺LT→AMG cells (green) and the location of the optrode (white). **i**, Optogenetic tagging (blue) of a PIL Calr⁺LT→AMG cell. **j**, Autocorrelogram (ACC; left) and waveforms (WF; right) of the same cell recorded with the four wires of a tetrode. **k**, Activity changes of the same cell evoked by sound presentations (shaded area) in each experimental session: before conditioning (Pre-Cond, CS– and CS+) and during cued fear retrieval (Retrieval CS– and CS+). **l**, Mean *z*-scored and normalized Calr⁺LT→AMG unit activity changes ($N = 18$ cells) across the 3-day-long experiment. The order of neurons is identical across the four trials and was determined by the earliest short-latency (<50 ms) response to Retrieval CS+. Arrowheads indicate the activity responses of the example cell in **i**–**k**.

were strongly modulated by NpHR-mediated optogenetic silencing of Calr⁺LT inputs. The AStr, similar to the classical striatal regions, can form a basal ganglia circuit with direct and indirect outputs through the substantia nigra pars lateralis and the lateral globus pallidus, respectively (Supplementary Fig. 10t–y). In summary, the Calr⁺LT cell population links—as a hub—sensory and motor events in affective behavioral actions throughout intra-amygdala, cortical and striatal circuits.

Discussion

Our collective results show that sensory (CS) and nociceptive (US) signals originating from the brainstem converge onto individual Calr⁺LT neurons and that fear conditioning potentiates CS-mediated responses in these neurons. Thus, CS–US associations can already take place at the level of the thalamus via individual Calr⁺LT cells that provide the amygdala, as well as the cortex and the striatum, with multimodal and plastic information necessary for adaptive memory formation and recall. These observations challenge the widely accepted concept that the LA is the first site of CS–US association.

Here, we provided multiple lines of evidence to indicate that Calr⁺LT cells do not simply relay single CS or US modalities, but compute associated and experience-dependent information (CS+US) before the LA.

First, our activity-dependent anatomical and in vivo electrophysiological results indicated that Calr⁺LT cells and their synaptic amygdala targets show larger activation to associated signaling than pure auditory or aversive processing.

Second, Calr⁺LT cells collect signals from brain regions involved in the sensory processing of different modalities. The auditory and multisensory IC, the visual and multimodal SC, the somatosensory Pr5 and the nociceptive PAG cells are among the subcortical regions that form synaptic contacts with Calr⁺LT neurons. Consequently, the Calr⁺LT→AMG route can contribute to hippocampus-independent contextual memory formation and retrieval[37]. Silencing this pathway not only prevented auditory-cued fear learning but also the establishment and recall of contextual fear memory. Furthermore, in humans and monkeys, a colliculo–pulvinar system forms behavior-relevant connections involved in fearful visual signaling with the LA[38,39]. The caudal and medial parts of the pulvinar were placed in the LA-projecting thalamus in mice[40], an area identical to the location of Calr⁺LT neurons, which raises the possibility that the Calr⁺LT→AMG route is responsible for affective visual processes in both humans and primates.

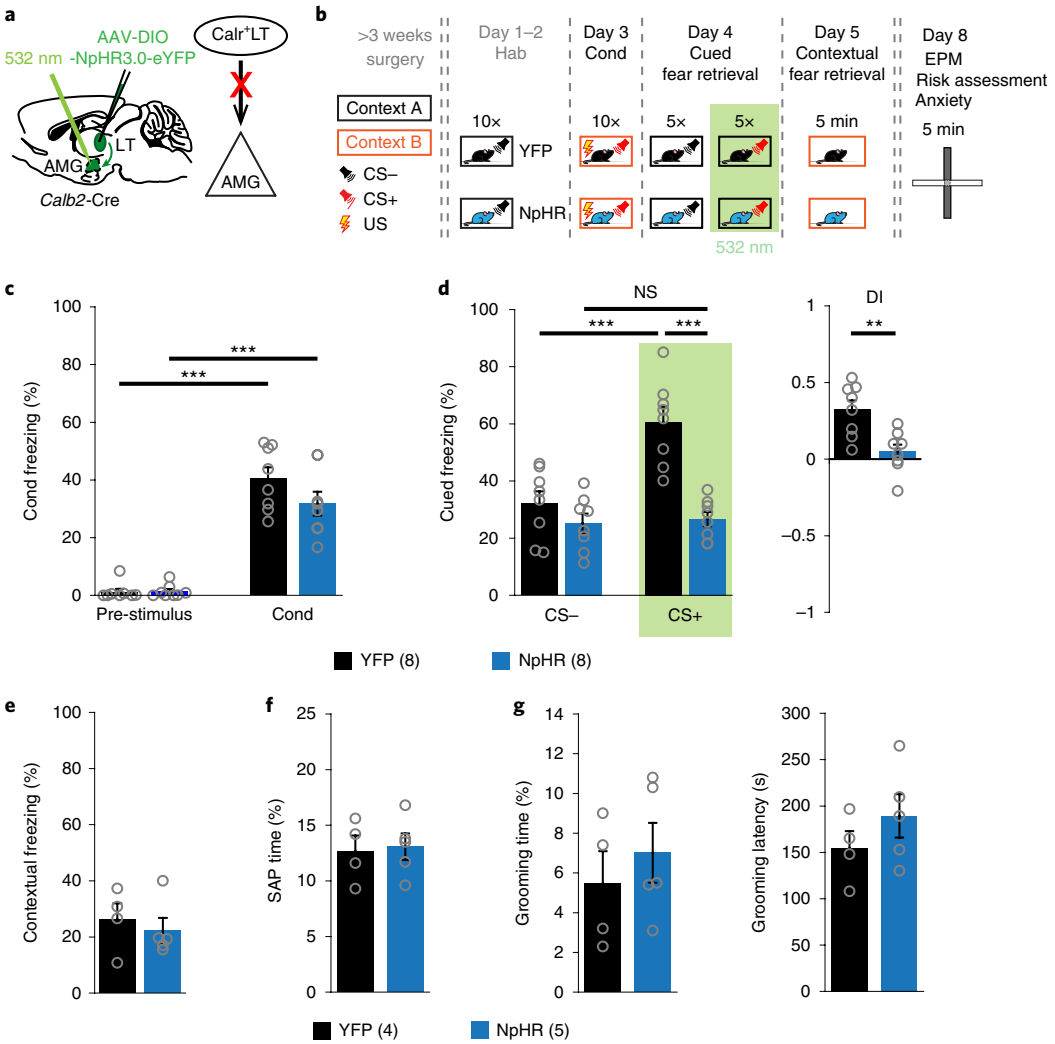

Fig. 8 | Calr⁺LT→AMG neurons control fear memory retrieval. a,**b**, Schematic (**a**) and behavioral protocol (**b**) for optogenetic silencing (green shading) of Calr⁺LT→AMG inputs during the CS+ presentation on the day of cued fear retrieval (see Methods). **c**, Freezing behavior during fear conditioning. Repeated-measures ANOVA group × time interactions ($F_{1,14}=2.531$, $P=0.134$); repeated-measures ANOVA for time ($F_{1,14}=155.5638$, $P<1\times10^{-6}$) with Tukey HSD test. **d**, Left: freezing behavior in cued fear retrieval. Repeated-measures ANOVA for group × time interactions ($F_{1,14}=22.4646$, $P=0.00032$) with Tukey HSD test. Right: calculated DI values. Mann–Whitney *U*-test (two-sided). **e**, Freezing in contextual fear retrieval. Mann–Whitney *U*-test (two-sided). **f**, Time spent in SAP during risk assessment. Mann–Whitney *U*-test (two-sided). **g**, Grooming behavior. Mann–Whitney *U*-test (two-sided). Data are shown as the mean ± s.e.m.; the number of mice are in parentheses next to the keys for the charts. $0.05<{}^{\#}P<0.1$, $^{*}P<0.05$, $^{*^{*}}P<0.01$, $^{***}P<0.001$. See Supplementary Table 5 for statistical details.

Third, the thalamus forms reciprocal connections with its corresponding cortical regions[41]. Calr⁺LT neurons do not project to the Au1, but preferentially target higher-order cortical regions like the AuV, the TeA and the insular cortex, which further suggests that these thalamic neurons are not directly involved in primary sensory processes. Sensory and higher-order cortical areas are crucial in associative learning[36] via a layer-1-mediated disinhibitory process[42]. Since higher-order cortical regions are innervated by Calr⁺LT neurons, with layer 1 receiving the densest axonal arbor, this thalamic population is in an ideal position to facilitate and maintain memory formation not only in the LA (recent and remote memory) but also in the neocortex (remote memory)[36].

Thalamic-input-mediated inhibitory and disinhibitory mechanisms, which play important roles in sensory gating during fear learning, have also been identified in the amygdala complex[30–33]. Our data show that the Calr⁺LT cells, which can elicit the above-mentioned cortical disinhibition, also have control over the GABAergic cells in the amygdala. Since the Calr⁺LT input can drive a fast and strong feedforward inhibition via SIC and LA interneurons, we suggest that it could also contribute to the enhancement of rhythmic amygdala activity. The tight connection to oscillation-generating amygdala networks might heavily contribute to the selection of competing amygdala cell ensembles that are further potentiated in affective learning[43,44].

Recalling LeDoux's theory about 'direct and indirect' thalamic routes to the amygdala[1], we identified the cellular source of these parallel pathways. The direct Calr⁺LT→AMG input can drive fast and robust evaluation and behavioral action in a dangerous situation, before any recognition. At the same time, sending collaterals to the AuV/TeA (which in turn provides strong cortical input to the LA), Calr⁺LT neurons can provoke cortical processes that are slower but more precise and involve consciousness.

In further signal processing, Calr$^+$LT and cortical inputs can spatially converge on amygdala cells[45]. Challenging the established idea of the coincident detection of separate CS and US inputs, we propose that CS+US-carrying Calr$^+$LT and cortical signals interact in the LA[46]. Summation of these inputs can then promote memory formation by driving NMDA-dependent plasticity at the LT→LA input[45,47] gated by inhibitory processes[30,31,33]. Furthermore, as the lateral thalamo–amygdala pathway (dominantly formed by Calr$^+$LT cells) also potentiates reward learning via NMDA- and/or AMPA-dependent changes[48,49], it is more than likely that these mechanisms of synaptic plasticity are also present at the Calr$^+$LT→AMG inputs. Finally, this thalamic input can also interact with neuromodulatory pathways in the amygdala[50]. Integrating all the above-noted cortical and subcortical signals, the amygdala can quickly select adaptive and adequate threat responses[6].

Altogether, our data suggest that the Calr$^+$LT→AMG population, transferring associated signals to the amygdala, cortical and basal ganglia networks, is in a unique position to develop and alter cue-related emotional behaviors.

Online content

Any methods, additional references, Nature Research reporting summaries, source data, extended data, supplementary information, acknowledgements, peer review information; details of author contributions and competing interests; and statements of data and code availability are available at https://doi.org/10.1038/s41593-020-0620-z.

Received: 12 August 2019; Accepted: 5 March 2020;
Published online: 13 April 2020

References

1. LeDoux, J. E. Emotion, memory and the brain. *Sci. Am.* **270**, 50–57 (1994).
2. Blair, H. T., Schafe, G. E., Bauer, E. P., Rodrigues, S. M. & LeDoux, J. E. Synaptic plasticity in the lateral amygdala: a cellular hypothesis of fear conditioning. *Learn. Mem.* **8**, 229–242 (2001).
3. Pape, H.-C. & Pare, D. Plastic synaptic networks of the amygdala for the acquisition, expression, and extinction of conditioned fear. *Physiol. Rev.* **90**, 419–463 (2010).
4. Nabavi, S. et al. Engineering a memory with LTD and LTP. *Nature* **511**, 348–352 (2014).
5. Weinberger, N. M. The medial geniculate, not the amygdala, as the root of auditory fear conditioning. *Hear. Res.* **274**, 61–74 (2011).
6. Headley, D. B., Kanta, V., Kyriazi, P. & Paré, D. Embracing complexity in defensive networks. *Neuron* **103**, 189–201 (2019).
7. Quirk, G. J., Repa, C. & LeDoux, J. E. Fear conditioning enhances short-latency auditory responses of lateral amygdala neurons: parallel recordings in the freely behaving rat. *Neuron* **15**, 1029–1039 (1995).
8. LeDoux, J. E., Farb, C. & Ruggiero, D. A. Topographic organization of neurons in the acoustic thalamus that project to the amygdala. *J. Neurosci.* **10**, 1043–1054 (1990).
9. LeDoux, J. E., Sakaguchi, A. & Reis, D. J. Subcortical efferent projections of the medial geniculate nucleus mediate emotional responses conditioned to acoustic stimuli. *J. Neurosci.* **4**, 683–698 (1984).
10. Campeau, S. & Davis, M. Involvement of subcortical and cortical afferents to the lateral nucleus of the amygdala in fear conditioning measured with fear-potentiated startle in rats trained concurrently with auditory and visual conditioned stimuli. *J. Neurosci.* **15**, 2312–2327 (1995).
11. Lanuza, E., Nader, K. & LeDoux, J. E. Unconditioned stimulus pathways to the amygdala: effects of posterior thalamic and cortical lesions on fear conditioning. *Neuroscience* **125**, 305–315 (2004).
12. Han, S., Soleiman, M. T., Soden, M. E., Zweifel, L. S. & Palmiter, R. D. Elucidating an affective pain circuit that creates a threat memory. *Cell* **162**, 363–374 (2015).
13. Johansen, J. P., Tarpley, J. W., LeDoux, J. E. & Blair, H. T. Neural substrates for expectation-modulated fear learning in the amygdala and periaqueductal gray. *Nat. Neurosci.* **13**, 979–986 (2010).
14. Kim, E. J. et al. Dorsal periaqueductal gray–amygdala pathway conveys both innate and learned fear responses in rats. *Proc. Natl Acad. Sci. USA* **110**, 14795–14800 (2013).
15. Penzo, M. A. et al. The paraventricular thalamus controls a central amygdala fear circuit. *Nature* **519**, 455–459 (2015).
16. Do-Monte, F. H., Quiñones-Laracuente, K. & Quirk, G. J. A temporal shift in the circuits mediating retrieval of fear memory. *Nature* **519**, 460–463 (2015).
17. Mátyás, F. et al. A highly collateralized thalamic cell type with arousal-predicting activity serves as a key hub for graded state transitions in the forebrain. *Nat. Neurosci.* **21**, 1551–1562 (2018).
18. Zhu, Y. et al. Dynamic salience processing in paraventricular thalamus gates associative learning. *Science* **362**, 423–429 (2018).
19. Bordi, F. & LeDoux, J. E. Response properties of single units in areas of rat auditory thalamus that project to the amygdala. II. Cells receiving convergent auditory and somatosensory inputs and cells antidromically activated by amygdala stimulation. *Exp. Brain Res.* **98**, 275–286 (1994).
20. Lanuza, E., Moncho-Bogani, J. & LeDoux, J. E. Unconditioned stimulus pathways to the amygdala: effects of lesions of the posterior intralaminar thalamus on foot-shock-induced c-Fos expression in the subdivisions of the lateral amygdala. *Neuroscience* **155**, 959–968 (2008).
21. Han, J.-H. et al. Increasing CREB in the auditory thalamus enhances memory and generalization of auditory conditioned fear. *Learn. Mem.* **15**, 443–453 (2008).
22. LeDoux, J. E., Ruggiero, D. A., Forest, R., Stornetta, R. & Reis, D. J. Topographic organization of convergent projections to the thalamus from the inferior colliculus and spinal cord in the rat. *J. Comp. Neurol.* **264**, 123–146 (1987).
23. Linke, R., De Lima, A. D., Schwegler, H. & Pape, H. C. Direct synaptic connections of axons from superior colliculus with identified thalamo-amygdaloid projection neurons in the rat: possible substrates of a subcortical visual pathway to the amygdala. *J. Comp. Neurol.* **403**, 158–170 (1999).
24. Coleman, J. R. & Clerici, W. J. Sources of projections to subdivisions of the inferior colliculus in the rat. *J. Comp. Neurol.* **262**, 215–226 (1987).
25. King, A. J. The superior colliculus. *Curr. Biol.* **14**, R335–R338 (2004).
26. Hayashi, H., Sumino, R. & Sessle, B. J. Functional organization of trigeminal subnucleus interpolaris: nociceptive and innocuous afferent inputs, projections to thalamus, cerebellum, and spinal cord, and descending modulation from periaqueductal gray. *J. Neurophysiol.* **51**, 890–905 (1984).
27. Bartlett, E. L., Stark, J. M., Guillery, R. W. & Smith, P. H. Comparison of the fine structure of cortical and collicular terminals in the rat medial geniculate body. *Neuroscience* **100**, 811–828 (2000).
28. Busti, D. et al. Different fear states engage distinct networks within the intercalated cell clusters of the amygdala. *J. Neurosci.* **31**, 5131–5144 (2011).
29. Grewe, B. F. et al. Neural ensemble dynamics underlying a long-term associative memory. *Nature* **543**, 670–675 (2017).
30. Asede, D., Bosch, D., Lüthi, A., Ferraguti, F. & Ehrlich, I. Sensory inputs to intercalated cells provide fear-learning modulated inhibition to the basolateral amygdala. *Neuron* **86**, 541–554 (2015).
31. Wolff, S. B. E. et al. Amygdala interneuron subtypes control fear learning through disinhibition. *Nature* **509**, 453–458 (2014).
32. Woodson, W., Farb, C. R. & LeDoux, J. E. Afferents from the auditory thalamus synapse on inhibitory interneurons in the lateral nucleus of the amygdala. *Synapse* **38**, 124–137 (2000).
33. Krabbe, S. et al. Adaptive disinhibitory gating by VIP interneurons permits associative learning. *Nat. Neurosci.* **22**, 1834–1843 (2019).
34. Almeida, T. F., Roizenblatt, S. & Tufik, S. Afferent pain pathways: a neuroanatomical review. *Brain Res.* **1000**, 40–56 (2004).
35. Cho, J.-H., Rendall, S. D. & Gray, J. M. Brain-wide maps of Fos expression during fear learning and recall. *Learn. Mem.* **24**, 169–181 (2017).
36. Sacco, T. & Sacchetti, B. Role of secondary sensory cortices in emotional memory storage and retrieval in rats. *Science* **329**, 649–656 (2010).
37. Zelikowsky, M., Bissiere, S. & Fanselow, M. S. Contextual fear memories formed in the absence of the dorsal hippocampus decay across time. *J. Neurosci.* **32**, 3393–3397 (2012).
38. Morris, J. S., Ohman, A. & Dolan, R. J. A subcortical pathway to the right amygdala mediating "unseen" fear. *Proc. Natl Acad. Sci. USA.* **96**, 1680–1685 (1999).
39. Rafal, R. D. et al. Connectivity between the superior colliculus and the amygdala in humans and macaque monkeys: virtual dissection with probabilistic DTI tractography. *J. Neurophysiol.* **114**, 1947–1962 (2015).
40. Zhou, N., Maire, P. S., Masterson, S. P. & Bickford, M. E. The mouse pulvinar nucleus: organization of the tectorecipient zones. *Vis. Neurosci.* **34**, E011 (2017).
41. Harris, J. A. et al. Hierarchical organization of cortical and thalamic connectivity. *Nature* **575**, 195–202 (2019).
42. Letzkus, J. J. et al. A disinhibitory microcircuit for associative fear learning in the auditory cortex. *Nature* **480**, 331–335 (2011).
43. Courtin, J., Karalis, N., Gonzalez-Campo, C., Wurtz, H. & Herry, C. Persistence of amygdala gamma oscillations during extinction learning predicts spontaneous fear recovery. *Neurobiol. Learn. Mem.* **113**, 82–89 (2014).

44. Amir, A., Headley, D. B., Lee, S.-C., Haufler, D. & Paré, D. Vigilance-associated gamma oscillations coordinate the ensemble activity of basolateral amygdala neurons. *Neuron* **97**, 656–669.e7 (2018).
45. Li, X. F., Stutzmann, G. E. & LeDoux, J. E. Convergent but temporally separated inputs to lateral amygdala neurons from the auditory thalamus and auditory cortex use different postsynaptic receptors: in vivo intracellular and extracellular recordings in fear conditioning pathways. *Learn. Mem.* **3**, 229–242 (1996).
46. Johnson, L. R. Hebbian reverberations in emotional memory micro circuits. *Front. Neurosci.* **3**, 198–205 (2009).
47. Weisskopf, M. G. & LeDoux, J. E. Distinct populations of NMDA receptors at subcortical and cortical inputs to principal cells of the lateral amygdala. *J. Neurophysiol.* **81**, 930–934 (1999).
48. Tye, K. M., Stuber, G. D., de Ridder, B., Bonci, A. & Janak, P. H. Rapid strengthening of thalamo-amygdala synapses mediates cue–reward learning. *Nature* **453**, 1253–1257 (2008).
49. Rich, M. T., Huang, Y. H. & Torregrossa, M. M. Plasticity at thalamo-amygdala synapses regulates cocaine-cue memory formation and extinction. *Cell Rep.* **26**, 1010–1020.e5 (2019).
50. Likhtik, E. & Johansen, J. P. Neuromodulation in circuits of aversive emotional learning. *Nat. Neurosci.* **22**, 1586–1597 (2019).

Methods

Nomenclature and nuclear boundaries. Nomenclature and nuclear boundaries are two critical points in brain research, especially in the case of the thalamus. There are no clear and strict borders between functionally distinct areas, so we applied a new concept to define territories in the lateral thalamic region. We considered input–output organizations and/or neurochemical markers to highlight thalamic territories[17,51–53]. Then, we correlated the results with atlases (The Mouse Brain by Paxinos and Franklin[54] or the one provided by the Allen Brain Institute, http://atlas.brain-map.org) and literature datasets. Calr$^+$ and LA-projecting thalamic cells are almost entirely overlapping, ~94% of the projecting cells contained Calr (Fig. 1d). Therefore, the Calr marker allowed us to clearly differentiate those regions that project to the LA and those that do not. To identify these thalamic areas, we used The Mouse Brain[54] because the classification in this atlas best matched the distribution of the Calr$^+$ thalamic cells.

The LA-projecting thalamic cells were clustered around the MGN. The dorsal cluster was located in the area of the SG based on The Mouse Brain atlas, and partially in the territory of the dorsal MGN (MGD). As the largest part of the MGN does not express Calr, and the Calr$^+$ and Calr$^-$ thalamic cells showed distinct connectivity patterns (Fig. 4b–d; Supplementary Fig. 9a–e), we decided to collectively call this dorsal cluster as SG cells. The ventral cluster almost entirely lay on the posterior intralaminar thalamic nucleus, abbreviated as PIL in The Mouse Brain, but also indicated as PIN, PIT, PoT (posterior triangular) and SPFp (parvocellular subparafascicular nucleus of the thalamus) in the literature (for example, see refs. [5,10,21,55–57]), in the Rat brain atlas by Swanson[58] (http://larrywswanson.com) as well as in the Allen Brain mouse atlas. Published data on rat also showed that the MGM[8] projects to the LA. We also found a few retrogradely labeled cells in this territory linking the dorsal and ventral clusters. As the MGM contained Calr$^+$ cells and the LA-projecting cells in this region were also Calr$^+$, we identified these as Calr$^+$ SG or PIL cells. We called all the above-mentioned clusters as the Calr$^+$ lateral thalamic ensemble, since their collicular inputs (Fig. 3) and their cortical and LA innervation were similar.

Although the term 'lateral thalamic' does not exist in the literature, it was chosen for a practical reason. The amygdaloid complex receives most of its thalamic afferents from two Calr$^+$ thalamic cell groups. One of them is located medially, including the paraventricular, intermediodorsal, centromedial and intralaminar thalamic nuclei, and it preferentially projects to the basolateral and centrolateral amygdala[17]. The other one is the population built-up by the above-described clusters of neurons, laterally and caudally to the medial Calr$^+$ group, and it sends input to the LA. Thus, for the purpose of clear distinction, we called the LA-projecting one the Calr$^+$LT cell ensemble. As this population resembles a higher-order thalamic nucleus regarding, for example, its connectivity, which is distinct from the first-order MGN, we decided to avoid using the terminology of 'Calr$^+$MGN'. In parallel, all the Calr$^-$ neurons located in these thalamic (PIL, SG and MGN) regions were collectively named Calr$^-$LT cells.

Experimental subjects. Adult (2–5 months old) *Calb2*-Cre, *vGat*-Cre, *vGlut2*-Cre (donated by Z. J. Huang, L. Acsády and S. Arthaud, respectively) and C57BL/6 mice of both sexes were used for the experiments. Only male mice were used in the behavioral assays, and littermates were randomly assigned to experimental groups. All animals were group-housed in a humidity- and temperature-controlled environment. They were entrained to a 12 h light–dark cycle (light phase from 7:00) with food and water available ad libitum. One week before the experiments, animals were individually housed and habituated to the experimenter (or experimenters) and to the test environment by handling for at least three times during their light phase. Testing also occurred during the light phase. All procedures were approved by the Regional and Institutional Committee of the Research Centre for Natural Sciences.

Generation of the AAV-DFO-ChR2-eYFP. The *ChR2-eYFP* coding sequence was cloned in-frame under the human synapsin (h*Syn*) promoter in the double-floxed forward open reading-frame (DFO) configuration, such that transcription can occur only in the absence of the Cre recombinase. In the presence of Cre, the transgene is reversed such that no transcription can occur. This configuration allowed the expression of the *ChR2-eYFP* transgene in Cre-negative cells and the exclusion from Cre-(Calb2)-positive cells.

Stereotactic surgeries. *AAV injection.* Mice were anesthetized using ketamine–xylazine (5:1, 3× dilution), and AAV-Ef1a-DIO-ChR2-eYFP, AAV-Ef1a-DIO-ChR2-mCherry, AAV-DIO-NpHR3.0-eYFP, AAV-DFO-ChR2-eYFP, AAV-DIO-eYFP and/or AAV-DIO-mCherry viruses (30–50 nl; Penn Vector Core or UNC; titer: $5\times10^{12}$to 1×10^{13} genome copies (GC) per ml) were injected at a rate of 0.5–1 nl s^{-1} into the following regions using a Nanoliter Injector (WPI): PIL/SG (anterior–posterior, lateral and dorsal–ventral (AP/L/DV) coordinates: −3.1/±1.9/3.3–2.8 mm); TeA/AuV (−3.2-3.6/4.5/1.5 mm); SC (−4/0.9/0.5–1 mm); IC (−5.1/1.5/0.5–0.8 mm); and LA (−1.8/3.5/3.8 mm). For the purpose of thalamic axon arbor analysis, after 3–6 weeks of survival time, mice were perfused.

Connectivity mapping. To identify the neurochemical nature of LT cells projecting to the LA and the AStr, single retrograde tracings were carried out using CTB (List Biological Laboratories, 104). To reveal the target selectivity of LT neurons, we performed double retrograde tracings with Alexa488-conjugated or Alexa555-conjugated CTB (Invitrogen) in the cases of LA/AStr and used a retro-anterograde viral approach in the cases of LA+AStr/TeA+AuV injections[17]. Native CTB was iontophoretically injected (7–7 s on/off duty cycle; 2–3 µA, for 10 min) in both male and female mice ($n=23$ in total), while the conjugated CTB (30 nl) was high-pressure injected with a Nanoliter Injector ($n=15$ mice). Animals injected with CTB were perfused after 1 week, while those with injected with AAVs were perfused after 4–6 weeks of survival time.

To reveal the projection pattern of the AStr and the SIC, we used 5% biotinylated dextran amine (BDA; molecular weight of 3,000, ThermoFisher, D1956). BDA was iontophoretically injected (2–2 s on/off, 2–3 µA, 5–10 min) into the AStr (AP/L/DV: −1.4/3.0/3.2 mm; $n=5$ mice) and the SIC (AP/L/DV: −1.4/3.2/–3.2 mm; $n=10$ mice). Animals were perfused after 1 week of survival time. The coordinates of the SIC were set according to the location of the neurons showing footshock-evoked c-Fos expression in the ventrolateral part of the AStr (dorsal to the ITC and LA, and medial to the LA). BDA injections that labeled neurons outside this 'corner' region resulted in no axonal labeling in the LA (Supplementary Fig. 10t–y). Mice with incorrect tracer injection(s) were excluded from the analysis ($n=31$).

Mono-trans-synaptic rabies tracing. The experimental design used in this paper has been used and validated in earlier studies[59,60]. *Calb2*-Cre mice ($n=3$) were injected with 50 nl of AAV2/8-hSynFLEX-TVA-p2A-eGFP-p2A-oG (4.5×10^{12} GC per ml) into the PIL/SG at the coordinates given above. After 3 weeks of survival, mice were injected with rabies(ΔG)-EnvA-mCherry (3.5×10^{7} GC per ml) at the same coordinates. After another 10 days of survival, mice were perfused. Both the rabies (mCherry) and the AAV (enhanced green fluorescent protein (eGFP)) signal were amplified with immunofluorescent staining (see later).

Unit recordings with chronically implanted optrodes. Calb2-Cre mice ($n=23$) were unilaterally injected with AAV-Ef1a-DIO-ChR2-eYFP into the amygdala. At 4–6 weeks after AAV injection, four custom-fabricated tungsten tetrodes (12.5 µm in diameter, California Fine Wire) were chronically implanted into the LT along with a multimode optic fiber (105-µm core diameter, NA = 0.22; Thorlabs), all tunneled in a polyimide tube (0.008 ID, Neuralynx). The tetrode wires were attached to an electrode interface board (EIB-16, Neuralynx) using gold electrode contact pins (Neuralynx). The ground and reference wires were soldered to the electrode interface board. Before implantation, tetrodes were cut to final length (200–400 µm left between the optic fiber and tetrode tips); impedances measured at 1 kHz were kept between 300 and 700 kΩ. Ground and reference screws were implanted in the occipital and parietal bones, accordingly. Finally, all pieces were secured onto the skull by multiple layers of dental acrylic (Paladur, Heraeus Kulzer) and shielded by a copper web. Mice were left for at least 7 days to recover and then handled for several days. Mice with incorrect virus injection or tetrode position were excluded from the analysis ($n=13$).

Optogenetic manipulations. Male *Calb2*-Cre mice ($n=107$) were bilaterally injected with AAV-Ef1a-DIO-NpHR3.0-eYFP or AAV-Ef1a-DIO-eYFP (for controls) into the LT. Immediately after AAV injections, multimode optic fibers (105-µm core diameter, NA = 0.22, Thorlabs) were bilaterally implanted above the LA, then fixed to the skull with dental cement. At 3–4 weeks, mice underwent the behavioral protocol starting with 3 days of handling.

Finally, all mice were transcardially perfused with saline, then with ~150 ml of fixative solution containing 4% paraformaldehyde dissolved in 0.1 M phosphate buffer (PB). Mice with incorrect virus injection(s), optic fiber implantation or US delivery failure during the fear-conditioning session were excluded from the analysis ($n=17$).

Tissue processing and immunohistochemistry. All the anatomical data, including those acquired with viral vectors, were obtained from immunohistochemically stained brain slices. No native signals were used for analysis, not even for eYFP, eGFP and mCherry proteins. Tissue blocks were cut using a Vibratome (Leica) into 50-µm coronal sections. Free-floating sections were intensively washed (5 times for 10 min) with 0.1 M PB. All antibodies were diluted in 0.1 M PB. For high-quality fluorescent labeling, sections were treated with a blocking solution containing 10% normal donkey serum (Abcam, 7475) or normal goat serum (Vector, S-1000) and 0.5% Triton-X in 0.1 M PB for 30 min at room temperature (RT). Then, sections were incubated in primary antibody solution at RT overnight or for 2–3 days (4 °C). The following primary antibodies were used: GFP (chicken, ThermoFisher Scientific, A10262; 1:2,000; rabbit, ThermoFisher Scientific, A11122; 1:10,000); mCherry (rabbit, BioVision, 5993-100; 1:2,000); Calr (mouse, Swant, 6B3; 1:1–3,000); FoxP2 (mouse, Merck Millipore, MABE415; 1:2,000); c-Fos (rabbit; Sigma, ABE457; 1:1,000); mGluR1α (guinea pig, Frontiers, Af660, RRID, AB_2571801; 1:500); calbindin (rabbit, Swant, CB-38a; 1:2,000); neuronal marker (NeuN; mouse, Merck Millipore, MAB377; 1:2,000); and CTB (goat; List Biological Laboratories, 703; 1:20,000). After primary antibody incubation, sections were treated with the following secondary IgG antibodies for fluorescent staining (1:500; 2 h at RT): Alexa 488-conjugated donkey anti-rabbit (Jackson ImmunoResearch, 711-545-152) and

donkey anti-mouse (Jackson ImmunoResearch: 715-545-150); Alexa 555-conjugated donkey anti-goat (Molecular Probes, A21432), donkey anti-mouse (Molecular Probes, A31570) and goat anti-chicken (Molecular Probes, A11309); Cy3-conjugated donkey anti-rabbit (Jackson ImmunoResearch, 711-165-152), donkey anti-mouse (Jackson ImmunoResearch, 715-165-151) and donkey anti-guinea pig (Jackson ImmunoResearch, 706-166-148); Alexa 594-conjugated donkey anti-mouse (Molecular Probes, A21203) and donkey anti-rabbit (Molecular Probes, A21207); Alexa 647-conjugated donkey anti-mouse (Jackson, 715-605-151) and donkey anti-rabbit (Jackson, 711-605-152). When necessary, staining was enhanced after primary antibody incubation with biotinylated secondary antibodies (biotinylated horse anti-mouse IgG, Vector Laboratories, BA-2000; 1:300; biotinylated goat anti-rabbit, Vector Laboratories, BA-1000; 1:300; 1.5 h at RT), Elite Avidin–Biotin Complex (eABC; 1:300, Vector Laboratories; 1.5 h at RT) and subsequently with streptavidin-conjugated fluorescent antibodies (SA-A488, Jackson ImmunoResearch, 016-540-084; 1:2,000; SA-Cy3, Jackson ImmunoResearch, 016-160-084; 1:2,000; SA-A647, Jackson ImmunoResearch, 016-600-084; 1:2,000; 2 h at RT). All fluorescent slices were mounted in Vectashield (Vector Laboratories).

Alternatively, we used DAB-Ni as a chromogen. Sections were treated first with 1% H_2O_2 solution (10 min), then incubated in 10% normal donkey serum/normal goat serum and 0.2% Triton-X solution as a blocking serum (30 min, RT). After primary antibody incubation, slices were incubated in biotinylated secondary antibodies (horse anti-mouse IgG or goat anti-rabbit) and eABC (see above). To visualize BDA, sections were incubated with eABC, then developed with DAB-Ni. Sections were then dehydrated in xylol and mounted in DePex (Serva).

Quantification of c-Fos expression. Neuronal activation in distinct phases of the fear-learning paradigm was monitored via c-Fos induction. The c-Fos antibody was developed with DAB-Ni (see above for details). All sections used for quantification were developed for the same duration. Three sections per animal were analyzed: one from the rostral, middle and caudal part of the LT or amygdala in each case, separated by 600 µm. The number of c-Fos-labeled cells in the LT and amygdala was determined using custom-written ImageJ and Matlab routines.

We used Calr$^+$ immunostaining to outline the thalamic and the amygdala nuclei. In the amygdala, the Calr$^+$ immunohistochemical staining showed intensity differences between the LA and the CeA, which could reflect the distinct quantity of the Calr protein in the afferent neuron terminals of different regions. Therefore, Calr$^+$ immunohistochemical staining could clearly distinguish the individual amygdala subnuclei.

c-Fos$^+$ cells were especially dense in a region laterally bounded by the LA, ventrally by the BA and the medial intercalated amygdala nucleus, medially by the CeA and dorsally by the AStr. This territory of c-Fos$^+$ neurons is introduced as the SIC and it is located AP between –1.3 and –1.8. It should be noted that it is unlikely that the SIC only contains US-activated and CS+US-activated LA-projecting and/or AStr-projecting cells. Rather, it is intermingled with AStr medium-spiny neurons.

Colocalization. To determine the proportion of Calr$^+$ neurons among the CTB-labeled or c-Fos-labeled LT populations, the mCherry/YFP coexpression in the LT as well as the vGAT-YFP/c-Fos coexpression in the SIC, we performed double fluorescent staining. *Z*-stack (step size: 5 µm) confocal images were taken with ×20–63 objectives (Zeiss, Olympus and Nikon) (4–5 slices per animals, $n=3$–5 animals). For Calr staining, due to the low penetration of the primary antibody, *Z*-stacks (step size: 2 µm) were taken only from the surface of the slices. In each experiment, colocalization was manually analyzed.

Estimation of the length of Calr$^+$LT and Calr$^-$LT axons. Calb2-Cre mice were unilaterally injected with a mixture of AAV-Ef1a-DIO-ChR2-mCherry and AAV-hSyn1-DFO-ChR2-eYFP viruses into the LT ($n=4$ mice). After 4 weeks, fluorescent labeling of the two viruses were amplified and the slices were counterstained for Calr to outline the borders of the amygdala subnuclei (Supplementary Fig. 4a). Confocal *Z*-stack (step size: 0.27 µm) images were taken with a ×63 objective. Two to three sections were analyzed in each animal. The length of Calr$^+$ (mCherry) and Calr$^-$ (YFP) axons was estimated using a custom-written Fiji macro[17] in a given region of interest. Finally, axonal length and density were calculated for the total volume per area in each animal. Grouped data showing the proportion of Calr$^+$ and Calr$^-$ axonal density are illustrated in Fig. 4d: LA Calr$^+$, 631,625 ± 313,822 µm (87.08 ± 6.56%); LA Calr$^-$, 80,923 ± 54,112 µm (12.92 ± 6.56%); AStr Calr$^+$, 364,525 ± 180,267 µm (83.41 ± 6.69%); AStr Calr$^-$, 62,956 ± 20,930 µm (16.59 ± 6.69%); caudate putamen (CPu) Calr$^+$, 39,489 ± 23,797 µm (16.95 ± 4.87%), CPu Calr$^-$, 193,528 ± 98,086 µm (83.05 ± 4.87%).

Electron microscopy. Combined immunogold–immunoperoxidase double immunostaining was performed to visualize the synaptic contacts formed by the collicular inputs arriving onto Calr$^+$LT neurons. Three weeks after the AAV-DIO-eYFP injection into the SC or the IC of *vGlut2*-Cre mice ($n=3$ for each region), the animals were perfused. All washing steps and the dilutions of antibodies and reagents were made with 0.1 M PB. After slicing and extensive washing (5 times for 10 min), the 50-µm-thick sections were incubated in 30% sucrose for 2 h, followed by freeze–thawing four times over liquid nitrogen. Then, the procedure included the following steps: blocking in 3% BSA for 45 min; incubation in the mixture of rabbit anti-GFP and mouse anti-Calr (1:3,000) primary antibodies overnight; incubation in biotinylated horse anti-mouse IgG (1:300; Vector Laboratories) for 2 h; incubation in avidin biotinylated-horseradish peroxidase complex (1:300; eABC; Vector Laboratories) for 1.5 h; blocking in 0.5% H_2O_2 for 10 min; amplification with Tyramide (Invitrogen, 1:50, 15 min); incubation for 1 h in blocking solution containing 0.5% human serum albumin and 0.1% CWFS (Aurion); overnight incubation in 0.8 nm gold-conjugated streptavidin (Aurion) solution (1:50) diluted in the same blocking solution at 4 °C; post-fixation in 2% glutaraldehyde for 15 min; silver intensification with Aurion R-Gent SE-EM kit for 60 min; incubation in anti-mouse ImmPRESS, (MP-5402; 1:2, Vector) for 2 h; preincubation in 0.025% DAB for 20 min; development with 0.5% H_2O_2 for 10–15 min; osmicated with 0.5% OsO_4 for 20 min at 4 °C; and finally dehydration, including treatment with 1% uranyl acetate diluted in 70% ethanol, for 40 min. Areas of interest were reembedded and sectioned for electron microscopy. Ultrathin (60 nm) serial sections were collected on Formvar-coated single slot grids. DAB-labeled axon terminals originating from the SC ($N=51$ boutons) and the IC ($N=43$ boutons) were identified, forming asymmetrical synapses onto immunogold-labeled Calr$^+$ postsynaptic elements.

In vivo electrophysiology in anesthetized preparations. In vivo recordings were performed 4–8 weeks after viral injections (AAV-DIO-ChR2-eYFP, AAV-DIO-NpHR3.0-eYFP) into the LT or the amygdala in *Calb2*-Cre mice. The head of the animal was fixed with a headplate in the stereotaxis frame, allowing acoustic stimulation of the ear contralateral to the recording site. A screw driven into the occipital bone served as a reference electrode. Thalamic ($n=10$ mice) and amygdala ($n=11$ mice) extracellular activities were monitored with 32-channel silicon probes (Buzsaki32, Neuronexus) stained with fluorescent DiI. Wideband neural data (0.1–7,500 Hz) were amplified (gain: 192×) and digitized at 20 kHz (Intan Technologies). We worked with two different recording conditions. The electrode ensemble and the optic fiber were lowered into either the amygdala or the LT, and orthodromic manipulations (Calr$^+$LT axonal inhibition and Calr$^+$LT somatic excitation, respectively) were done locally. Alternatively, in the case of LT recordings, the optic fiber was positioned in the amygdala and the fibers of Calr$^+$LT neurons were activated so that antidromic-evoked responses could be detected in the LT. The amygdala does not contain Calr$^+$ cells projecting back to the LT, so thalamic responses were due to direct antidromic activation. Optogenetic activation consisted of 473-nm blue-light pulses (5 ms, 0.5–1 Hz, ~15 mW, Laserglow Technologies), which served only for the identification of Calr$^+$LT neurons.

Auditory and footshock-evoked responses were also tested in the thalamus and the amygdala subnuclei. Auditory signals were composed of 7.5 kHz pure tones (1 s, 75 dB), while footshock stimulation was achieved by bipolar electric stimulation (50 or 100 ms, 1 mA) of a foot, which resulted in pain reflex. The two types of cues were also paired to form a multimodal associated signal. Unimodal auditory and foot shock, as well as associated stimuli, were repeated 10 times in thalamic recordings, and 50, 10 and 20 times, respectively, in amygdala recordings, keeping 2–5-min interblock intervals. Interstimulus intervals (ISIs) were 40–60 s. The lasers, speakers and the current generator (Medicor) were triggered by analog (lasers and speakers) or digital (current generator) signals driven by a National Instruments acquisition board (USB-6353) and Matlab. Analog trigger pulses were also delivered to the recording system and registered in parallel with neural data with zero latency.

For the amygdala recordings, optogenetic axonal inhibition[61] was done with 532-nm green-laser stimuli (continuous 5 s, 15–20 mW; Laserglow Technologies) to silence Calr$^+$LT signal transmission in the amygdala during sensory stimulation. Blocks of sensory stimulations overlapping with Calr$^+$LT axonal inhibition were alternating with stimulations without silencing. The effect of NpHR-driven inhibition on spontaneous amygdala neuronal firing was also tested with 30 s of continuous illuminations.

After recordings, animals were transcardially perfused, and coronal sections were cut from the paraformaldehyde-fixed brains. The position of the silicon probe was verified after DiI labeling of the electrode track. Mice with incorrect virus injection or electrode position were excluded from the analysis ($n=9$).

Unit recordings from freely behaving mice during auditory fear learning. During the behavioral paradigm, the interface board was connected to an Intan recording system via a 16-channel RHD 2132 preamplifier (Intan Technologies; gain: 192×; sampling frequency: 20 kS s^{-1}; frequency range: 0.1–7,500 Hz). The optogenetic laser was triggered by a National Instruments board (USB-6343) controlled by Matlab. Analog trigger pulses were registered in parallel with the neural data. The behavior of mice was captured on video at 30 frames per s.

Optogenetic taggings were performed in the homecage, then, mice were placed in the behavioral apparatus. Laser stimulation was repeated before and after the behavioral tests. Optogenetic tagging of Calr$^+$LT cells was done with 5-ms long, low-intensity (473-nm laser intensity was set to <1 mW for orthodromic and 5–6 mW for antidromic stimulations) laser pulses at 0.5 or 1 Hz. The applied lower laser intensity used here can be explained by the difference in response probability

between the anesthetized and the freely moving preparations. Higher laser intensities can also obstruct the unequivocal clustering of single units recorded in freely moving conditions.

Auditory stimuli were composed of 30-s-long continuous or 1-Hz pulse-trains of 7.5-kHz sinus wave (CS+) and Gaussian white noise (CS–). Mice underwent two habituation days (ten CS– in context A), one conditioning (four unpaired CS+ presentations followed by ten CS+ terminated by a foot shock (US, 1 mA, 1 s) in context B) and one retrieval day (five CS– and five CS+ in context A).

Neural data processing. Following noise filtering by average subtraction, raw electrophysiological recordings were filtered (>500 Hz) for spike detection. Spike detection and principal-component-analysis-based automatic clustering were performed using SpikeDetekt and KlustaKwik, respectively[62]. Cell grouping was manually refined using KlustaViewa. A group of spikes was considered to be generated by a single neuron if they formed a discrete, well-isolated cluster and had an autocorrelogram with a refractory period (if average bin values of the first 2 ms did not reach the autocorrelogram's asymptote line). We excluded cells in cases when they shared a symmetric cross-correlogram with units from different tetrodes as well as a similar shaped action potential to avoid enumerating the same cell more than once. In the case of optrode recordings, neuronal data from subsequent days were sorted together. Further data analyses were carried out using custom-built Matlab routines. All the presented electrophysiological data are derived from individually identified single units (clustered cells).

Short-latency (≤10 ms) light-evoked spiking was considered reliable to indicate direct light activation, thus enabling the identification of the Calr^{+}LT cell type. These neurons were chosen following a criterion of a z-scored spike rate above 3.3 ($P > 0.001$) in the first 10 ms after light onset. Every thalamic cell (within the PIL and SG regions as well as in their vicinity) showing weaker or no photoactivation was considered to be a Calr^{-}LT cell.

Significant evoked responses to auditory and footshock stimuli were defined for each sorted cell as follows. A Poisson-distribution-based confidence interval ($P < 0.05$) was set for a 1-s-long baseline before stimulations. If the mean of short-latency (<50 ms) and long-latency (<500 ms) post-stimulus spike count distribution exceeded this interval, and the signal-to-noise ratio (defined as the mean/s.d. ratio of spike rate) was not less than 0.5 in the case of short-term responses, cells were considered responsive. Only a few sensory-evoked inhibitory responses were found, which might be partially attributed to low baseline firing rates found in the PIL/SG and amygdala neurons (1.35 and 0.55 Hz on average, respectively), which compromises the detection of short-term decreases in spiking activity. Latency of responses was calculated after a 2.5-ms binning in the peri-stimulus time histogram, estimated as the first bin value larger than 3.3 in the z-scored peri-stimulus time histogram. Multilinear enhancement in short-latency and long-latency (see above) multimodal responses were defined as the increase in the average tone+footshock-evoked firing rate expressed as the percentage of the most likely unimodal (tone or footshock) response's mean firing rate[63]. For cases in which no unimodal response was present, but multisensory stimulation evoked significant changes in the firing rate, these were also considered enhanced/augmented activities.

Significant changes of evoked responses during thalamic axonal inhibition were validated using the same Poisson-distribution-based method.

Putative principal neurons (GABAergic medium-spiny neurons and glutamatergic LA neurons) and GABAergic LA interneurons as well as SIC were separated by their trough-to-peak spike-width, which we considered as the most reliable parameter for this purpose. SIC were identified as units on the electrode shanks placed above the dorsomedial intercalated neuronal region. Based on previous data on cortical GABAergic interneurons[64] and the bimodal distribution of amygdala neuronal spike-width (see Supplementary Fig. 5e), we distinguished SIC and LA interneurons by their trough-to-peak width that were equal to or less than 0.6 ms.

Behavioral paradigms. Following a series of handling, mice were tested in various environments (open-field chamber, conditioning box, EPM; MKI Plexi). Delivery of foot shock (Ionflow Bipolar, Supertech) and auditory stimulations were controlled by a National Instruments board (USB-6343) and custom-written Matlab codes. Behavioral tests were captured on video (30 frames per s). Mouse behavior was manually analyzed by an experimenter blinded to the group assignment of the animal (but not to the light conditions due to the visibility of optical stimulation) and quantified by the time/time percentage/count of freezing, rearing, escape behavior (jumping) and grooming using the software H77 recorder[65] (courtesy of J. Haller, Institute of Experimental Medicine).

c-Fos experiments. All mice (male *Calb2*-Cre) were habituated to context A (experimental box with dotted walls) and the unconditioned tone (CS–; white noise; 10×30 s) for two consecutive days (days 1–2).

The ISIs were pseudorandomly varied between 30 and 60 s in every case of auditory stimulation. The test cage was cleaned with 30% ethanol between animals.

Fear conditioning c-Fos. The following groups of animals ($n = 4$–5) were tested on the conditioning day (day 3) in context B (box with plain walls). (1) The absolute control group (Ctrl) received no stimulus during the 10 min spent in the experimental chamber. (2) The CS+ group received only tones (10×30 s 7.5 kHz). (3) The US group received only the US, foot shock (10×1 s 1 mA). (4) The CS+US group received conditioned tones (CS+, 10×30 s, 7.5 kHz), which were terminated with a foot shock (10×1 s, 1 mA; US).

Cued fear retrieval c-Fos. The following groups of animals were tested in context A after 2 days of habituation (CS–). (1) The pre-Retr. group received CS+US conditioning on day 3 and the animals were perfused 24-h later without being tested in retrieval. This group was used to set the maximum baseline c-Fos level after prior conditioning. (2–3) The CS-only groups were only given CS+ (10×30 s) during the conditioning day (day 3) without any US, and the next day, they received either five CS– or five CS+. (4–5) The CS+US groups received conditioned tones that were terminated with the US on day 3 and either CS– or CS+ on day 4. All animals were perfused 60 min after the experiments.

To Identify the GABAergic nature of the SIC showing footshock-induced c-Fos expression, *vGat*-Cre mice ($n = 4$ for each experiment) were injected with AAV-DIO-eYFP, and the protocols of control and US group were repeated.

Optogenetic silencing of behavior. Open-field test. The effect of Calr^{+}LT→AMG axonal silencing on spontaneous behavior was measured in an open-field chamber (40 cm×40 cm×40 cm). Optogenetic stimulation was carried out with a 532-nm green laser (Laserglow Technologies) at 15–20 W intensity.

The first minute served as an acclimatization phase, which was followed by a 6-min testing period: 6×30 s of continuous 532-nm light illuminations (on periods) were alternating with 30 s of off periods. The proportion of freezing behavior and the relation of center versus periphery location were compared between animals with and without laser illumination.

Cued and contextual fear conditioning. Mice were subjected to a single-trial auditory fear-conditioning paradigm and received optogenetic silencing only once (Supplementary Fig. 6c). Two different contexts were used: context A with dotted walls and context B with plain walls.

On day 1–2 (habituation) in context A, a 90-s pre-stimulus interval (PSI) was followed by 10×30 s of continuous CS– (75 dB Gaussian white noise) presentations with pseudorandom 30–60-s-long interleaving (ISI).

On day 3, during auditory fear conditioning (day 3) in context B, the 90 s of PSI was followed by 10×30 s of continuous CS+ (75 dB, 7.5 kHz pure tone) terminated with a US foot shock (1 s, 1 mA), with 30–60 s of ISI. The group of CS-only YFP mice received CS+ without the US. Green-laser illumination was delivered in each YFP and NpHR group for either the entire length of the CS+ only/CS+US presentation (30 s; Fig. 6c,d) (conditioning NpHR silencing) or the last 5 s of CS+ overlapping the US presentation (US NpHR silencing; Supplementary Fig. 6c,f). Freezing during the tone presentations (30 s) was compared to the PSI period.

On day 4, cued fear-memory discrimination was tested in context A. After 90 s of PSI, mice were given 5 repetitions of 30 s of CS– and CS+, subsequently with 30–60 s of ISI. In the cued fear-retrieval NpHR silencing assay, CS+ presentations were paired with light stimulation (30 s; Fig. 8) in both the YFP and NpHR mice. The fear discrimination index (DI) was calculated from time percentages of freezing during CS–/CS+ using the following equation: $DI = (freezing_{CS+} - freezing_{CS-}) / (freezing_{CS+} + freezing_{CS-})$.

On day 5, in context B, contextual fear memory was tested for 5 min. In the contextual fear-retrieval NpHR silencing assay, 90 s of PSI was followed by an alternation of 6×30 s of continuous light illuminations (on periods) with 30 s of off periods. Freezing during the light periods were compared between NpHR and YFP groups.

Anxiety and risk assessment test. Three days after the contextual fear test (day 8), an EPM equipment was used without any laser stimulation to determine any long-term behavioral effect caused by Calr^{+}LT axonal inhibitions during the conditioning or cued fear-retrieval days. The maze was made of gray-painted Plexiglas and consisted of two open arms (30×7 cm) and two closed arms (30×7 cm with 30-cm high walls), which were connected by a central platform (7×7 cm). The plus-maze was elevated to 70 cm above the floor. Mice were placed on the central platform facing one of the open arms and were allowed to explore the apparatus for 5 min. The total number of entries was calculated to measure locomotor activity, while the ratio of closed-arm versus open-arm time was given as an anxiety measure[66]. Mice were considered to enter a compartment when all their four legs crossed the virtual lines separating the compartments. Risk-assessment activities were analyzed based on those described by Rodgers and Dalvi[67]. We scored the latency and duration of grooming behavior as well as the parameters of the stretch–attend posture (an exploratory posture in which mice elongate their body and then retract it without any forward locomotion).

Statistical analysis. Data in the figures represent the mean ± s.d. or the mean ± s.e.m. as indicated in the figure legends. The number of analyzed cells is shown with N, while n represents the number of animals. Data from independent experiments were pooled when possible. No statistical methods were used to predetermine sample sizes. Sample sizes were chosen based on earlier experiments[15–17] to appropriately detect statistical significance, considering

technical feasibility and ethical animal use. Statistical significance was assessed using two-tailed *t*-tests or Mann–Whitney *U*-tests based on the normality level of the dataset, as well as analysis of variance (ANOVA). Normality was tested using the Kolmogorov–Smirnov test. χ^2 tests were used to compare the distribution of responsive LT and amygdala cells. Statistical analysis was performed using Statistica 13 (Statsoft) or Matlab. Significance levels are indicated as follows: $0.1 > {}^{\#}P > 0.05$; $^{*}P < 0.05$; $^{**}P < 0.01$; $^{***}P < 0.001$; $^{****}P < 0.0001$; NS, not significant.

Reporting Summary. Further information on experimental design is available in the Nature Research Reporting Summary linked to this article.

Data availability

Data from this study as well as material from custom products are available from the corresponding author upon request.

Code availability

Custom-written codes used to analyze data from this study are available from the corresponding author upon request.

References

51. Kim, S., Matyas, F., Lee, S., Acsady, L. & Shin, H.-S. Lateralization of observational fear learning at the cortical but not thalamic level in mice. *Proc. Natl Acad. Sci. USA* **109**, 15497–15501 (2012).
52. Mátyás, F., Lee, J., Shin, H.-S. & Acsády, L. The fear circuit of the mouse forebrain: connections between the mediodorsal thalamus, frontal cortices and basolateral amygdala. *Eur. J. Neurosci.* **39**, 1810–1823 (2014).
53. Cai, D. et al. Distinct anatomical connectivity patterns differentiate subdivisions of the nonlemniscal auditory thalamus in mice. *Cereb. Cortex* **29**, 2437–2454 (2018).
54. Paxinos, G. & Franklin, K. B. J. *The Mouse Brain in Stereotaxic Coordinates* (Academic Press, 2003).
55. Quirk, G. J., Armony, J. L. & LeDoux, J. E. Fear conditioning enhances different temporal components of tone-evoked spike trains in auditory cortex and lateral amygdala. *Neuron* **19**, 613–624 (1997).
56. Gauriau, C. & Bernard, J.-F. A comparative reappraisal of projections from the superficial laminae of the dorsal horn in the rat: the forebrain. *J. Comp. Neurol.* **468**, 24–56 (2004).
57. Lipshetz, B. et al. Responses of thalamic neurons to itch- and pain-producing stimuli in rats. *J. Neurophysiol.* **120**, 1119–1134 (2018).
58. Swanson, L. W. *Brain Maps: Structure of the Rat Brain* (Elsevier Academic Press, 2004).
59. Szőnyi, A. et al. Brainstem nucleus incertus controls contextual memory formation. *Science* **364**, eaaw0445 (2019).
60. Wickersham, I. R. et al. Monosynaptic restriction of transsynaptic tracing from single, genetically targeted neurons. *Neuron* **53**, 639–647 (2007).
61. Mahn, M., Prigge, M., Ron, S., Levy, R. & Yizhar, O. Biophysical constraints of optogenetic inhibition at presynaptic terminals. *Nat. Neurosci.* **19**, 554–556 (2016).
62. Rossant, C. et al. Spike sorting for large, dense electrode arrays. *Nat. Neurosci.* **19**, 634–641 (2016).
63. Meredith, M. A. & Stein, B. E. Visual, auditory, and somatosensory convergence on cells in superior colliculus results in multisensory integration. *J. Neurophysiol.* **56**, 640–662 (1986).
64. Barthó, P. et al. Characterization of neocortical principal cells and interneurons by network interactions and extracellular features. *J. Neurophysiol.* **92**, 600–608 (2004).
65. Mikics, É., Barsy, B., Barsvári, B. & Haller, J. Behavioral specificity of non-genomic glucocorticoid effects in rats: effects on risk assessment in the elevated plus-maze and the open-field. *Horm. Behav.* **48**, 152–162 (2005).
66. Walf, A. A. & Frye, C. A. The use of the elevated plus maze as an assay of anxiety-related behavior in rodents. *Nat. Protoc.* **2**, 322–328 (2007).
67. Rodgers, R. J., Cao, B.-J., Dalvi, A. & Holmes, A. Animal models of anxiety: an ethological perspective. *Braz. J. Med. Biol. Res.* **30**, 289–304 (1997).

Acknowledgements

We thank Z. J. Huang, L. Acsády and S. Arthaud for providing us with transgenic mice, C. Porrero and F. Clascá for their instructions for BDA injections, N. Holderith for sharing primary antibodies, Cs. Dávid for advising us on axonal analysis and A. Szőnyi for rabies injections. The technical assistance of K. Varga, V. Kanti, J. Berczik, A. Fehér, L. Truka, R. Pop and E. Szabó-Együd in histology is acknowledged. We wish to thank the Institute of Enzymology at RCNS, Nikon Microscopy Center at IEM, Nikon Austria and the Auro-Science Consulting for kindly providing microscopy, as well as the Institute of Materials and Environmental Chemistry at RCNS for technical support. We thank L. Acsády, N. Bunford, T. L. Horváth, M. Penzo and I. Soltész for comments and discussions about the manuscript. This work was supported by the National Office for Research and Technology (FK124434 and KKP126998 to F.M., PD124034 to B.B., and FK129120 to D.H.), by the Hungarian Brain Research Program (grant numbers KTIA-NAP-13-2-2015-0010 to F.M., and 2017-1.2.1-NKP-2017-00002 to F.M. and I.U.), by the New National Excellence Program of the Ministry for Innovation and Technology (ÚNKP-19-3-III-PPKE-68 to K.K., and ÚNKP-19-4-ÁTE-8 to F.M.), by the Széchenyi 2020 Program, the Human Resource Development Operational Program, the Program of Integrated Territorial Investments in Central-Hungary (EFOP-3.6.2-16-2017-00013 and 3.6.3-VEKOP-16-2017-00002 to K.K. and I.U.; EFOP-3.6.2-16-2017-00012 to F.M.), by the Adelis Foundation (O.Y.), and by the European Research Council (ERC CoG 819496 to O.Y.). F.M. is a János Bolyai Research Fellow.

Author contributions

B.B., K.K., I.U. and F.M. designed the experiments. B.B., K.K., Á.B., A.M., J.M.V. and F.M. performed animal surgeries, immunocytochemistry and confocal analyses. B.B. and M.S. conducted behavioral experiments and analyses. K.K. and A.M. performed in vivo electrophysiological recordings and data analyses. O.Y. developed the AAV-DFO plasmid, and D.H. produced the AAV-DFO viral vector. B.B., K.K. and F.M. wrote the manuscript, which was edited by all authors.

Competing interests

The authors declare no competing interests.

Additional information

Supplementary information is available for this paper at https://doi.org/10.1038/s41593-020-0620-z.

Correspondence and requests for materials should be addressed to F.M.

Peer review information *Nature Neuroscience* thanks Fabricio H. do Monte and the other, anonymous, reviewer(s) for their contribution to the peer review of this work.

Reprints and permissions information is available at www.nature.com/reprints.

nature research

Corresponding author(s): Ferenc Matyas

Last updated by author(s): Feb 11, 2020

Reporting Summary

Nature Research wishes to improve the reproducibility of the work that we publish. This form provides structure for consistency and transparency in reporting. For further information on Nature Research policies, see Authors & Referees and the Editorial Policy Checklist.

Statistics

For all statistical analyses, confirm that the following items are present in the figure legend, table legend, main text, or Methods section.

n/a	Confirmed	
☐	☒	The exact sample size (*n*) for each experimental group/condition, given as a discrete number and unit of measurement
☐	☒	A statement on whether measurements were taken from distinct samples or whether the same sample was measured repeatedly
☐	☒	The statistical test(s) used AND whether they are one- or two-sided *Only common tests should be described solely by name; describe more complex techniques in the Methods section.*
☒	☐	A description of all covariates tested
☐	☒	A description of any assumptions or corrections, such as tests of normality and adjustment for multiple comparisons
☐	☒	A full description of the statistical parameters including central tendency (e.g. means) or other basic estimates (e.g. regression coefficient) AND variation (e.g. standard deviation) or associated estimates of uncertainty (e.g. confidence intervals)
☐	☒	For null hypothesis testing, the test statistic (e.g. *F*, *t*, *r*) with confidence intervals, effect sizes, degrees of freedom and *P* value noted *Give P values as exact values whenever suitable.*
☒	☐	For Bayesian analysis, information on the choice of priors and Markov chain Monte Carlo settings
☒	☐	For hierarchical and complex designs, identification of the appropriate level for tests and full reporting of outcomes
☐	☒	Estimates of effect sizes (e.g. Cohen's *d*, Pearson's *r*), indicating how they were calculated

Our web collection on statistics for biologists contains articles on many of the points above.

Software and code

Policy information about availability of computer code

Data collection	Zeiss ZEN 2010B SP1 Release version 6.0 (Carl Zeiss Microimaging GmbH) RHD2000 Interface Software v1.4.2 (Intan Technologies)
Data analysis	ImageJ 1.52i (Fiji) MATLAB (versions 2014a, 2016a, 2018a and 2019a) klusta 3.0.15 Statistica 13 (Statsoft) H77 (custom-written event recorder, József Haller, Budapest; Mikics et al., 2005, Hormones and Behavior)

For manuscripts utilizing custom algorithms or software that are central to the research but not yet described in published literature, software must be made available to editors/reviewers. We strongly encourage code deposition in a community repository (e.g. GitHub). See the Nature Research guidelines for submitting code & software for further information.

Data

Policy information about availability of data

All manuscripts must include a data availability statement. This statement should provide the following information, where applicable:

- Accession codes, unique identifiers, or web links for publicly available datasets
- A list of figures that have associated raw data
- A description of any restrictions on data availability

All data obtained in this study are available from the corresponding author upon reasonable request.

Field-specific reporting

Please select the one below that is the best fit for your research. If you are not sure, read the appropriate sections before making your selection.

☒ Life sciences ☐ Behavioural & social sciences ☐ Ecological, evolutionary & environmental sciences

For a reference copy of the document with all sections, see nature.com/documents/nr-reporting-summary-flat.pdf

Life sciences study design

All studies must disclose on these points even when the disclosure is negative.

Sample size	No statistical methods were used to predetermine sample sizes. Sample sizes were chosen based on earlier experiments (Do Monte et al., 2015, Nature; Penzo et al., 2015, Nature, Mátyás et al., 2018, Nature Neuroscience) in order to appropriately detect statistical significance, also considering technical feasibility and ethical animal use.
Data exclusions	All data from animals with incorrect viral/tracer injections or electrode/optic fiber positions were excluded from data analysis.
Replication	To ensure that experimental findings can be easily reproduced, we included detailed methods and sources of all reagents and protocols for the experiments included in the manuscript. All behavioral experiments were repeated with the number of mice specified in the manuscript. Individual data points and error bars were presented in the figures. All electrophysiological data were collected from the specified number of cells. All histological and microscopic analysis were repeated with at least 2-3 mice. Exact sample sizes are provided in the figure legends or in the supplementary tables.
Randomization	All subjects were randomly assigned to groups.
Blinding	In all behavioral experiments investigators were blinded to allocation and outcome assessments except those with optogenetic manipulations due to the visibility of optical stimulation. All other experiments and their analyses were performed in blinded manner.

Reporting for specific materials, systems and methods

We require information from authors about some types of materials, experimental systems and methods used in many studies. Here, indicate whether each material, system or method listed is relevant to your study. If you are not sure if a list item applies to your research, read the appropriate section before selecting a response.

Materials & experimental systems

n/a	Involved in the study
☐	☒ Antibodies
☒	☐ Eukaryotic cell lines
☒	☐ Palaeontology
☐	☒ Animals and other organisms
☒	☐ Human research participants
☒	☐ Clinical data

Methods

n/a	Involved in the study
☒	☐ ChIP-seq
☒	☐ Flow cytometry
☒	☐ MRI-based neuroimaging

Antibodies

Antibodies used

Primary antibodies:
Chicken polyclonal anti-GFP (ThermoFisher Scientific: A10262, Lot#1917944), 1:2000
(https://www.thermofisher.com/antibody/product/GFP-Antibody-Polyclonal/A10262)

Rabbit polyclonal anti-GFP (ThermoFisher Scientific: A11122, Lot#1965877), 1:10000
(https://www.thermofisher.com/antibody/product/GFP-Antibody-Polyclonal/A-11122)

Rabbit polyclonal anti-mCherry (BioVision: 5993-100, Lot# 2H235993), 1:2000
(https://www.biovision.com/documentation/datasheets/5993.pdf)

Mouse monoclonal anti-Calretinin (Swant: 6B3, Lot# 010399), 1:1-3000
(https://www.swant.com/pdfs/Monoclonal_calretinin_6B3.pdf)

Mouse monoclonal anti-FoxP2 (Merck Millipore: MABE415 clone FOXP2-73A/8, Lot#2789404), 1:2000
(https://www.merckmillipore.com/HU/hu/product/Anti-FoxP2-Antibody-clone-FOXP2-73A-8,MM_NF-MABE415)

Rabbit polyclonal anti-cFos (Sigma: ABE457, Lot#2905394), 1:1000
(https://www.sigmaaldrich.com/catalog/product/mm/abe457?lang=hu&region=HU)

Guinea Pig polyclonal anti-mGluR1α (Frontier Inst. Co.: Af660; RRID : AB_2571801), 1:500
(https://www.frontier-institute.com/wp/wp-content/uploads/pdf/mGluR1a.pdf)

Rabbit polyclonal anti-Calbindin (Swant: CB-38a, Lot# 9.03), 1:2000
(https://www.swant.com/pdfs/Rabbit_anti_calbindin_D-28k_CB38.pdf)

Mouse polyclonal anti-Neuronal Marker (NeuN) (Merck Millipore: MAB377, Clone A60, Lot#2639366), 1:2000
(https://www.merckmillipore.com/HU/hu/product/Anti-NeuN-Antibody-clone-A60,MM_NF-MAB377)

Goat polyclonal anti-Cholera Toxin B subunit (List Biological Laboratories: 703, Lot#7032A9), 1:20000
(https://www.listlabs.com/products/buy-anti-cholera-toxin-b-subunit-goat)

Fluorescent Secondary antibodies (1:500):
Alexa Fluor 488 conjugated AffiniPure Donkey anti-Rabbit IgG (Jackson ImmunoResearch:711-545-152, Lot#135979)
Alexa Fluor 488 conjugated AffiniPure Donkey anti-Mouse IgG (Jackson ImmunoResearch:715-545-150, Lot# 120901)
Alexa Fluor 555 conjugated Donkey anti-Goat IgG (Molecular Probes: A21432, Lot#1697092)
Alexa Fluor 555 conjugated Donkey anti-Mouse IgG (Molecular Probes: A31570, Lot#1774719)
Alexa Fluor 488 conjugated Goat anti-Chicken IgG (Molecular Probes: A11309, Lot# 1691381)
Cy3 conjugated AffiniPure Donkey anti-Rabbit IgG (Jackson ImmunoResearch: 711-165-152, Lot#123091)
Cy3 conjugated AffiniPure Donkey anti-Mouse IgG (Jackson ImmunoResearch: 715-165-151, Lot#123025)
Cy3 conjugated AffiniPure F(ab')2 Donkey anti-Guinea Pig IgG (Jackson ImmunoResearch: 706-166-148, Lot#120628)
Alexa Fluor 594 conjugated Donkey anti-Mouse IgG (Molecular Probes: A21203, Lot#1722995)
Alexa Fluor 594 conjugated Donkey anti-Rabbit IgG (Molecular Probes: A21207, Lot# 1744751)
Alexa Fluor 647 conjugated Donkey anti-Mouse IgGJackson ImmunoResearch: 715-605-151 Lot#122180
Alexa Fluor 647 conjugated Donkey anti-Rabbit IgG Jackson ImmunoResearch: 711-605-152 Lot#123104

Biotinylated secondary antibodies (1:300):
Biotinylated Horse anti-Mouse IgG – bHAM (Vector Laboratories: BA-2000, Lot# Y0907)
Biotinylated goat anti-rabbit – bGAR (Vector Laboratories: BA-1000, Lot# Z0619)

Fluorescent Conjugated streptavidin (1:2000):
Alexa 488-conjugated streptavidin (Jackson ImmunoResearch: 016-540-084, Lot# 120825)
Cy3-conjugated streptavidin (Jackson ImmunoResearch: 016-160-084, Lot#122297)
Alexa 647-conjugated streptavidin (Jackson ImmunoResearch 016-600-084, Lot#121307)

Immuno Gold Conjugated streptavidin (1:50):
0.8 nm gold-conjugated streptavidin (Aurion, Lot# STR-60815/1)

Validation

The specificity of the primary antibodies was validated by the manufacturer. For details, please, see the manufacturer's website. Specificity of the secondary antibodies was confirmed by verifying a lack of expression in tissue sections in which the primary antibody was omitted from the immunohistochemical protocol.

Animals and other organisms

Policy information about studies involving animals; ARRIVE guidelines recommended for reporting animal research

Laboratory animals

Adult (2-5 months old) mice were used from both sexes in all experiments except behavioral assays in which only male mice were included.
Calb2-Cre (The Jackson Laboratory; #010774) donated by Z. Josh Huang
vGAT-Cre (The Jackson Laboratory; #016962) donated by László Acsády
BAC-vGluT2-Cre donated by Sébastien Arthaud
C57BL/6J (Charles River)

Wild animals

This study did not involve wild animals.

Field-collected samples

This study did not involve samples collected from the field.

Ethics oversight

National Animal Research Authorities of Hungary and Institutional Committee of the Research Centre for Natural Sciences.

Note that full information on the approval of the study protocol must also be provided in the manuscript.